Hydrological and Dynamical Characteristics of Summertime Droughts over U.S. Great Plains

FONG-CHIAU CHANG

Earth System Science Center, University of Alabama—Huntsville, NASA–UAH Global Hydrology and Climate Center, Huntsville, Alabama

ERIC A. SMITH

NASA Marshall Space Flight Center, NASA–UAH Global Hydrology and Climate Center, Huntsville, Alabama

(Manuscript received 11 August 1999, in final form 12 July 2000)

ABSTRACT

A drought pattern and its time evolution over the U.S. Great Plains are investigated from time series of climate divisional monthly mean surface air temperature and total precipitation anomalies. The spatial pattern consists of correlated occurrences of high (low) surface air temperature and deficit (excess) rainfall. The center of maximum amplitude in rain fluctuation is around Kansas City; that of temperature is over South Dakota. Internal consistency between temperature and precipitation variability is the salient feature of the drought pattern. A drought index is used to quantify drought severity for the period 1895–1996. The 12 severest drought months (in order) during this period are June 1933, June 1988, July 1936, August 1983, July 1934, July 1901, June 1931, August 1947, July 1930, June 1936, July 1954, and August 1936. Hydrological conditions are examined using National Centers for Environmental Prediction (NCEP) reanalysis precipitable water (PW) and monthly surface observations from Kansas City, Missouri, and Bismarck, North Dakota, near the drought centers. This analysis explains why droughts exhibit negative surface relative humidity anomalies accompanied by larger than normal monthly mean daily temperature ranges and why maximum PWs are confined to a strip of about 10° longitude from New Mexico and Arizona into the Dakotas and Minnesota.

Dynamical conditions are examined using NCEP reanalysis sea level pressures and 500- and 200-mb geopotential heights. The analysis indicates a midtroposphere wave train with positive centers situated over the North Pacific, North America, and the North Atlantic, with negative centers in the southeastern Gulf of Alaska and Davis Strait. Above-normal sea level pressures over New Mexico, the North Atlantic, and the subtropical Pacific along with below-normal sea level pressures over the Gulf of Alaska eastward to Canada, Davis Strait, and Greenland are present during drought periods. The most prominent feature is the strong anticyclone over central North America.

On a regional scale, midtropospheric westerly winds are weakened (or become easterly) south of a thermal heat low centered in South Dakota during drought episodes because of the north–south temperature reversal perturbation. The associated westward displaced Bermuda high leads to enhanced low-level warm flow into the Dakotas, thus helping to maintain the reversal in the meridional temperature gradient and the concomitant thermal wind reversal. Enhanced moisture transport from the Gulf of California into the western plains (part of the Great Basin monsoon process) results from the large-scale perturbation pressure pattern. Middle-upper level convergence maintains the water vapor strip east of the Rocky Mountains, while the Mississippi valley undergoes moisture cutoff from both this process and the westward shift in the Bermuda high. The strip of maximum PW then undergoes enhanced solar and infrared absorption that feeds back on the thermal heat low. Surface air temperatures warm while sinking motion balances middle-upper level radiative cooling around the Kansas City area. This is the dynamical coupling that leads to reduced surface relative humidities. The centers of high surface air temperature and deficit rainfall are dynamically consistent with patterns in geopotential heights, vertical velocities, and water vapor amounts.

1. Introduction

Summertime droughts over the U.S. Great Plains with their combination of high surface air temperatures and prolonged deficit rainfall severely affect the balance between water resources and demands. Atmospheric processes, sea surface temperature anomalies, and land surface conditions are all involved in their onset and persistence. This study examines 1) how Great Plains droughts are manifest at the global scale down to the regional scale, 2) how they emerge in a preferred spatial pattern, and 3) how they are maintained thermodynamically, dynamically, and hydrologically.

Kerr (1989) reviewed the scientific debate concerning whether the 1988 North American drought was the result

Corresponding author address: Dr. Fong-Chiau Chang, No. 12, Lane 220 Chung-Ho Road, Chung-Li, Taiwan 320.
E-mail: fongchiau_chang@yahoo.com

of an amplified greenhouse effect or natural variability. Although various GCMs indicate that the earth is getting warmer and the arid zones are moving north stemming from elevated concentrations of absorbing trace gases, there is evidence that Great Plains droughts are naturally recurrent phenomena (Rasmusson 1997). The linkage between the strong La Niña in 1988 (mature El Niño 1993) to the 1988 spring–summer drought (1993 summer floods) over North America highlights a teleconnection between climatic conditions over the equatorial Pacific and the U.S. Great Plains (Trenberth and Guillemot 1996).

Trenberth et al. (1988) suggested that the 1988 drought was primarily forced by changes in sea surface temperature (SST) in the equatorial Pacific and an associated northward-displaced intertropical convergence zone (ITCZ) in the eastern tropical Pacific. Trenberth and Branstator (1992) further emphasized that the primary ''instigators'' (their term) for the 1988 drought were diabatic heating anomalies over the subtropical eastern Pacific associated with a shift in the ITCZ. They noted that the observed wave train across North America was forced by these heating anomalies (also Ting and Wang 1997). Their conclusion was supported by several GCM experiments. These experiments produced anomalous circulation patterns similar to observations when the model was initialized for an early spring and run with observed SST anomalies (Palmer and Brankovic 1989; Kalnay et al. 1990). Other observational studies of mid- and upper-tropospheric circulation anomalies during droughts over the Great Plains focus on the importance of underlying dynamical processes (e.g., Klein 1952; Namias 1982, 1991; Chang and Wallace 1987).

Even though their modeling results indicate that SST anomalies over the open ocean are the primary precursor to Great Plains droughts, Trenberth and Branstator (1992) could not exclude the importance of land surface processes in the persistence of the 1988 North American drought. Koster and Suarez (1995) and Betts et al. (1996) showed that the influence of land surface processes on warm season precipitation variations is as important as SST anomalies. Also, simulations with the Goddard Laboratory for Atmospheres GCM model (using prescribed 1988 soil moisture anomalies) performed by Atlas et al. (1993) produced an increase in temperature and a reduction in precipitation over the Great Plains.

In a simplified two-dimensional rigid-walled modeling study of the African Sahel, Charney (1975) suggested that high surface albedos lead to elevated radiative cooling followed by enhanced sinking motion and precipitation reduction. However, in a subsequent study, Charney et al. (1977) indicated that land surface albedo–precipitation interactions were not that straightforward. In fact, in a set of related regional modeling experiments sensitive to surface fluxes, Sud and Fennessy (1982) noted that, for the U.S. Great Plains, elevated surface albedos can lead to reduced aridity.

Such results suggest a complex of surface factors is important for drought maintenance over the Great Plains, all linked to convective precipitation, which is the primary summertime rainfall mechanism in this region (Rasmusson 1968; Mintz 1984). Clearly, more refined observational and modeling studies are needed to understand the so-called biogeophysical feedback mechanism.

A few studies have addressed summertime droughts in the Great Plains over many decades. Palmer (1965) documented drought episodes over western Kansas during the 1887–1962 period, central Iowa during 1930–62, and northwestern North Dakota during 1931–62, making use of a drought severity index together with extensive excerpts from the *Weekly Weather and Crop Bulletin, Monthly Weather Review,* and other publications. Palmer's study provides evidence of the role of land surface hydrological processes in accounting for the persistence of drought episodes in the 1930s and 1950s.

Following Palmer's work, Chang and Wallace (1987), henceforth CW87, surveyed droughts in the Kansas City area during the 1889–1980 period (92 yr), along with the associated large-scale circulation patterns and land-surface moisture conditions. Their results corroborated that dynamical and hydrological processes work in tandem to produce summertime droughts in the Kansas City area, noting that drought months are characterized by 1) negative anomalies in relative humidity, 2) negative Palmer Drought Severity Index (PDSI), 3) upper-level anticyclones over the central United States, 4) enhanced surface anticyclones and upper-level ridges over oceans, 5) deeper-than-normal upper-level troughs along the west coast of North America, 6) deeper-than-normal surface lows over the Rocky Mountains, and 7) low temperatures over the Pacific Northwest.

There were months such as June 1952, July 1955, and June 1963 when hydrological conditions were normal with the anomalous circulation primarily responsible for hot weather. In other months, such as those in the summers of 1934, 1936, and 1954, soil conditions were anomalously dry, while sea level pressure patterns were not typical of hot months. There were months such as July 1935 and July 1980 when none of the statistics presented in their paper appear to be consistent with the hot weather observed at Kansas City. These ambiguities underlie the complex dynamical and hydrological linkages involved in a drought's initiation, maintenance, and termination.

In the present study, an important drought pattern and its time evolution over the U.S. Great Plains are investigated from time series of climate divisional summer (June–August) monthly mean surface air temperature and precipitation anomalies during the 1895–1996 period. Temperature and precipitation records are obtained from *Climate Division Temperature–Precipitation–Drought Data,* compiled by the National Climatic Data Center. Each climate division is located entirely within

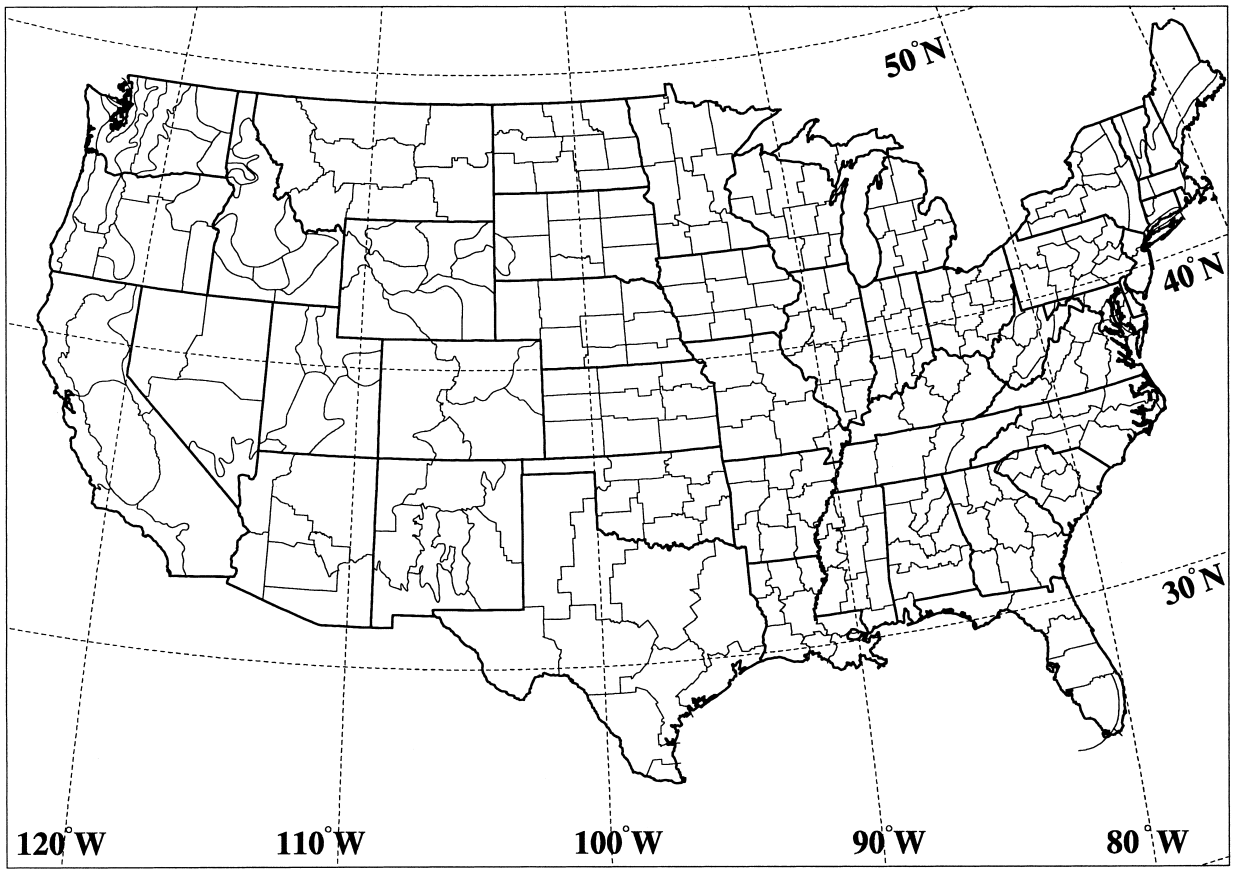

FIG. 1. Schematic map of 344 climate divisions (indicated with lighter lines) in the continental United States.

a single state as portrayed in Fig. 1. The divisional mean temperature for a particular month is obtained by averaging the maximum and minimum temperatures recorded at the climate network stations within the division. The bias due to the observer reporting time is corrected using the model described by Karl et al. (1986). This ''time bias–corrected'' scheme has been described in NCDC (1994).

TABLE 1. List of first 15 warmest and coolest months at Kansas City (39°N, 95°W) along with associated temperature anomalies (T − A).

Month	Yr	T − A (°C)	Month	Yr	T − A (°C)
Jun	1952	5.0	Aug	1915	−4.5
Aug	1936	4.9	Jul	1891	−4.1
Jun	1934	4.8	Jul	1950	−4.1
Jul	1934	4.8	Aug	1927	−3.8
Jul	1936	4.4	Jun	1928	−3.6
Aug	1947	4.4	Aug	1950	−3.4
Jun	1953	4.4	Jun	1945	−3.2
Jul	1954	4.0	Jun	1903	−3.2
Jul	1901	4.0	Jul	1895	−3.1
Aug	1913	4.0	Jul	1905	−3.0
Jun	1933	3.9	Aug	1974	−2.9
Jul	1935	3.9	Jul	1924	−2.9
Jun	1911	3.4	Jul	1915	−2.9
Jul	1955	3.1	Aug	1893	−2.8
Aug	1937	3.1	Jun	1951	−2.8

The National Centers for Environmental Prediction (NCEP) reanalysis of sea level pressures (SLP), both 500- and 200-mb geopotential heights, and precipitable water (PW) is used to examine dynamical processes and their relationship to drought maintenance. Hydrological conditions are examined using monthly surface observations from Kansas City, Missouri, and Bismarck, North Dakota. Monthly surface parameters include maximum and minimum temperatures, temperature, dewpoint, relative humidity, and precipitation. These data were obtained from back issues of the *Monthly Weather Review* (1889–1949) and *Climatological Data* (1950–80) [published by the National Climatic Data Center, National Oceanic and Atmospheric Administration (NOAA), Department of Commerce]. Climatological means for 1889–1980 were calculated for each individual month for each parameter. These long-term means were then used for the calculation of anomalies to be discussed in Tables 1–6.

Summertime teleconnectivities are calculated based on NCEP reanalysis SLPs and are presented in section 2. In section 3, the Kansas City surface air temperature anomaly record is analyzed to determine its character-

istic fluctuations with dominant periodic signals extracted using singular spectrum analysis. Section 4 examines the relationship between temperature and precipitation, and section 5 describes the dynamical and hydrological characteristics of summertime droughts over the U.S. Great Plains. Section 6 provides the main conclusions. The results show that Great Plains droughts are part of a large-scale atmospheric teleconnection, exhibit a preferred drought severity pattern, and are regulated by a linked set of meteorological processes involving the thermal wind, radiative cooling, and vertical motion.

2. Summertime sea level pressure teleconnection

Subtropical tropospheric stationary waves during summer exhibit a monsoonal character, with anomalies of opposite sign occurring in the 200-mb geopotential height and SLP (Wallace 1983). Deep cumulus convection and tropical-type weather systems become mainstays of summertime energetics (Holopainen 1970). Planetary waves produce a larger fractional contribution to the variance in the 1000-mb height field than in the 500-mb height field (White 1980). Hence, it is useful to calculate a teleconnectivity map based on NCEP reanalysis SLPs for investigating dynamical processes in drought initiation and maintenance.

The NCEP–National Center for Atmospheric Research (NCAR) reanalysis (Kalnay et al. 1996) was produced using a frozen 1994 state-of-the-art analysis-forecast system (i.e., a system that remains unchanged except for observing systems) and with data assimilation using past data from 1957 to present. The NCEP reanalysis system consists of the NCEP Medium Range Forecasting (MRF) spectral model (Kanamistu et al. 1991), which is a T62 28-level version of the global spectral model. The analysis module of the data assimilation system incorporates a spectral statistical interpolation scheme (Parrish and Derber 1992; Kalnay et al. 1996), effectively a three-dimensional variational analysis scheme. Geophysical parameters are available on a 2.5° lat–long grid on a daily or monthly basis.

Here, we have calculated SLP teleconnectivity for every NCEP grid point over the Northern Hemisphere using the first released NCEP reanalysis product. The data series length is 39 summer months (June–August) from the 1982–94 record. Following Wallace and Gutzler (1981), we use the ''negative extrema'' technique, a conceptually simple method but with lengthy calculations. The procedure is 1) calculate correlation between a base grid point and every other grid point over domain (Northern Hemisphere), 2) assign strongest negative correlation from above calculation as teleconnectivity of a base grid point, 3) construct correlation map indicating teleconnectivity for every grid point, and 4) connect base grid points that exhibit greatest teleconnectivity to grid points that exhibit strongest negative correlations.

The resultant teleconnectivity map shown in Fig. 2 reveals that 1) the North Atlantic oscillation involves a seesawing in SLP between the Davis Strait and the North Atlantic, while 2) the North Pacific oscillation involves a seesawing in SLP between the North Pacific and Aleutians. Other pairings include 3) the Eastern North Pacific and Norwegian Sea, 4) Denmark and the Greenland Sea, and 5) the Gulf of Alaska and New Mexico. Note the last pairing has received little attention in the literature.

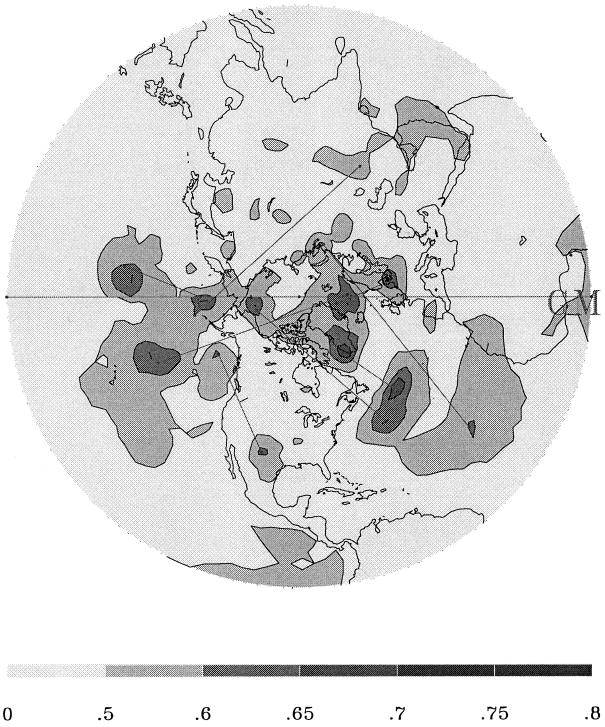

FIG. 2. Summertime SLP teleconnectivity map over Northern Hemisphere. Teleconnectivity of any grid point is the strongest negative correlation between SLP at given grid point and every other grid point over the Northern Hemisphere. Regions where teleconnectivities exceed 0.5 are shaded. Solid lines connect base grid points that exhibit greatest teleconnectivity to grid points that exhibit strongest negative correlation over northern hemisphere. Results are based on 39 summer months, i.e., all Jun–Aug months for 1982–94 period (13 yr).

Noteworthy, the linkage in SLP fluctuations between New Mexico and the Gulf of Alaska exhibits the influences of the fluctuations of the North American monsoon strength on summertime climate variations. Douglas et al. (1993) defined a monsoon index (MI) as the ratio (expressed in percent) of rain falling during the 3-month period July–September to the annual mean precipitation. They found the maximum values of MI are over the region surrounding the southern Gulf of California extending along the axis of the Sierra Madre Occidental into southeastern Arizona, and north and northeastward along the Rio Grande valley in New Mexico. Douglas (1995) suggested that moisture transported from the eastern Pacific by the low-level jet over the Gulf of California contributes to the abrupt increase in

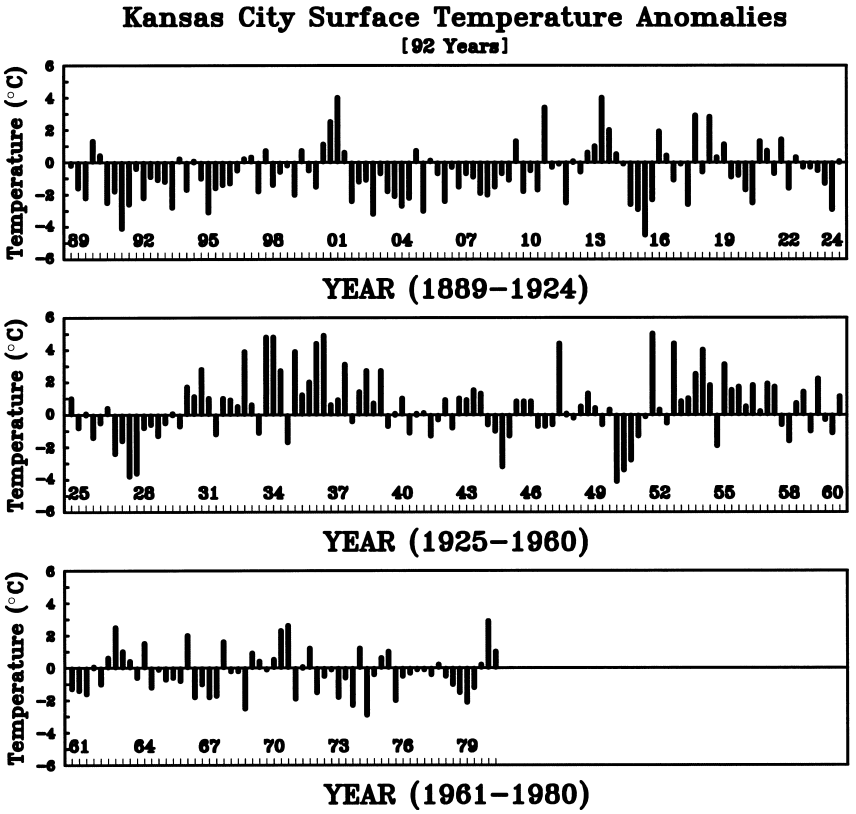

FIG. 3. Time series of summer monthly mean surface air temperature anomalies at Kansas City during the 1889–1980 period (92 yr).

rainfall over the southwestern United States. Above-normal SLP over New Mexico and below-normal SLP over the Gulf of Alaska will enhance the lower-level pressure gradient over Baja California, the Gulf of California, and Sonora. This enhanced pressure gradient, in turn, strengthens the low-level jet over the Gulf of California and moisture transport into southwestern North America. In addition, the westward extension of the Bermuda high cuts off water vapor transport from the Gulf of Mexico to the Mississippi valley while forcing more northward warm surface airflow from the northern Mexico–U.S. Southwest region onto the high plains.

3. Surface air temperature anomalies at Kansas City

In considering whether the 1988 North American drought was the result of an amplified greenhouse effect, it is useful to ask if there is any long-term trend in the 92-yr Kansas City surface air temperature anomaly record. Figure 3 shows the time series of summer monthly mean surface air temperature anomalies at Kansas City during 1889–1980. Most conspicuous in this 276-month time series is the clustering of hot and cool years. Extremely hot years are clustered in the 1930s and 1950s, a multidecadal-type fluctuation. Cool years span 1891–96, 1902–08, 1923–28, and 1950–51. Some argue that variations of solar irradiance associated with sunspot activity (i.e., the equatorial propagating sunspot cycle) are an important mechanism contributing to terrestrial temperature change (Lean and Rind 1998). Long-term sun–moon—weather–climate relationships have also been pointed out by Currie (1979) and Stockton and Meko (1983) from long-term tree-ring records. Several studies indicate relationships among sunspot activity, the quasi-biennial oscillation, and temperature variability (Labitzke 1987; Labitzke and van Loon 1992). In this section we examine periodic signals embedded in the 92-yr Kansas City normalized surface air temperature anomaly record (1889–1980).

As shown in Nicolis and Nicolis (1984, 1986), a climate system eventually reaches an attractor when the transients die out. Based on this idea, Broomhead and King (1986) and Vautard and Ghil (1989) have shown that singular spectrum analysis (SSA) can effectively identify periodic signals in noisy and short-term climate time series. In essence, the technique uses objective time filters to separate dominant albeit sometimes low-amplitude oscillations in a given time series. We utilized SSA to extract dominant oscillations from the 92-summer surface air temperature anomaly record at Kansas City.

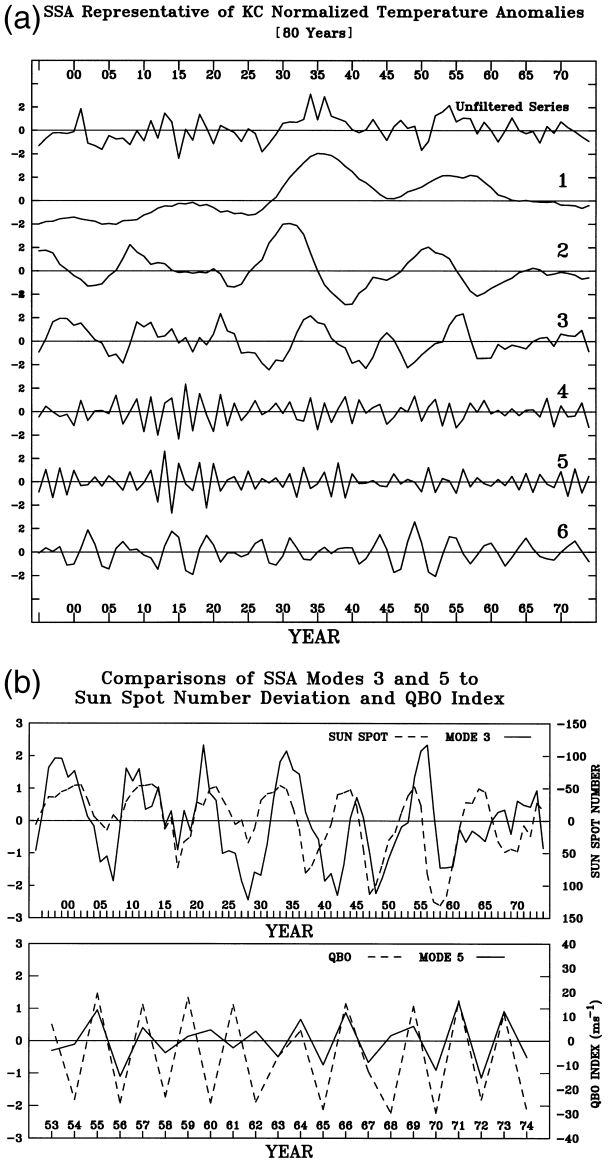

FIG. 4. (a) Unfiltered time series (top curve) and time evolution of first six modes (in order from second–seventh curves) extracted from singular spectrum analysis of 92-yr summer mean surface air temperature anomalies at Kansas City. (b) (top) Third mode extracted from singular spectrum analysis of 92-yr summer mean surface air temperature anomalies at Kansas City (solid line) overlaid with sunspot number perturbation (dashed line) based on normal created by averaging Jun, Jul, Aug monthly sunspot numbers for 80 yr. (bottom) The same result for fifth mode overlaid with QBO index (based on stratospheric winds since 1953).

Figure 4a shows the first six modes along with the normalized time series for 1895–1974. Note the SSA analysis is based on a 12-yr embedding dimension, which truncates the first and last 6-yr periods, yielding a normalized time series of 80 yr. Possible evidence for the sun's effect on drought appears in various modes. The first mode explains 21.5% of the variance and shows an oscillation with a period of about 19–20 yr that is multidecadal but also may contain power related to the period of the sun's 22-yr Hale cycle, during which the magnetic poles of the sun and sunspot polarity flip and return to their original orientation. The second mode (16%) exhibits an oscillation with a period of about 17.5 yr and is nominally multidecadal. The third mode (10.5%) shows an approximate 11.5-yr cycle, consistent with the sun's 11-yr sunspot propagation cycle and one-half of a Hale cycle. This mode is plotted separately in the upper panel of Fig. 4b along with the sunspot number perturbation for the same period; the two time series are in close agreement. Thus, the first and third modes suggest an underlying natural variation associated with solar irradiance variability, as espoused in the work of Dr. Judith Lean and her colleagues over the last decade, while the second decadal-type mode may be related to slow modification of internal surface boundary conditions over either land or ocean.

The fourth and sixth modes (7.0% and 6.2%) exhibit periodicities of about 2.5 and 5.25 yr, suggesting relationships to the irregular cycle associated with El Niño–Southern Oscillation (ENSO) whose repeat cycle typically varies from 3 to 5 yr. The fifth mode (6.8%), of which a truncated portion is shown separately in the lower panel of Fig. 4b, exhibits a periodicity of about 2.3 yr nearly mimicking the cycle of the 2.2-yr quasi-biennial oscillation (QBO). The QBO index, based on stratospheric winds for the period after 1953, is overlaid on the Fig. 4b lower panel to show it is in phase with the fifth mode since the inception of the QBO index record [see Naujokat (1986) and Piexöto and Oort (1992) for a discussion of the standard QBO record]. A biennial oscillation in surface air temperature over the United States was also pointed out by Rasmusson et al. (1981).

Overall, periodicities associated with solar activity, internal oscillations coupling the ocean–land surface and atmosphere, dynamical coupling between stratosphere and troposphere, and other multidecadal processes appear as the dominant mechanisms modulating Great Plains droughts. The only noticeable long-term trends are exhibited in the first mode, indicating an upward trend from 1895 to 1935 and downward trend from 1935 to 1974. This suggests natural variability is the major control on Great Plains drought episodes as opposed to a slowly intensifying greenhouse process, however, time series analysis by itself cannot validate or invalidate causality.

4. Time evolution of drought pattern

a. Relationships between temperature and precipitation

Prolonged episodes of abnormal moisture deficit represent the main feature of drought. From a surface hydrological viewpoint, antecedent soil moisture (on a timescale of a few months) and current precipitation

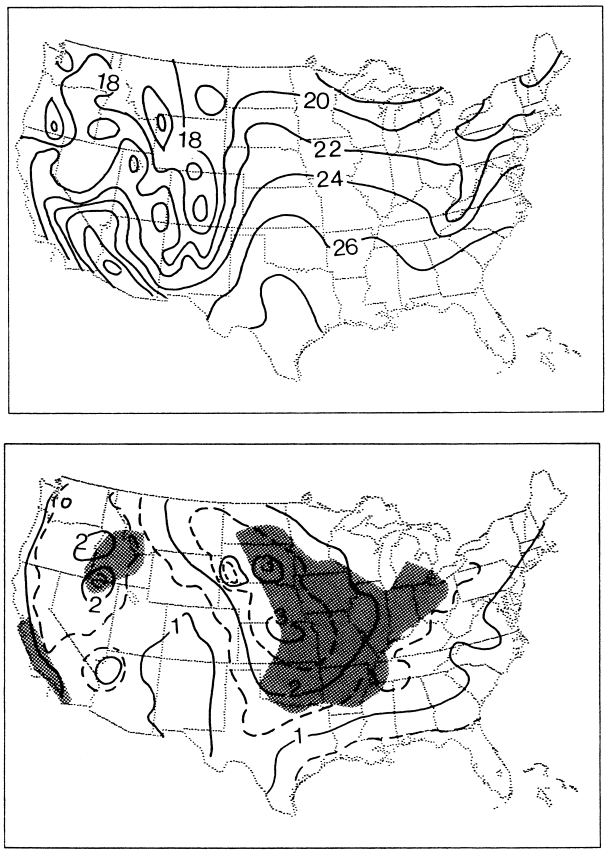

FIG. 5. (top) Climatological mean summer monthly mean surface air temperatures during 1931–82 period (52 yr); contour interval is 2°C. (bottom) Variance of summertime monthly mean surface air temperatures; contour interval is 0.5°C^2. Shaded area indicates that skewness moment of 156-month temperature distribution is greater than 0.3.

represent the moisture supply. Prolonged episodes of moisture deficit occurred simultaneously with episodes of high surface air temperature in the Great Plains during the 1930s, 1952–54, and 1988 droughts. Since temperature and precipitation are interrelated, climatological statistics of these two parameters are important in interpreting the underlying dynamical and hydrological processes of droughts. Here we present statistics adapted from Chang (1986). They are based on 156 summer months from the 1931–82 record.

Climatological mean summer monthly surface air temperatures are presented in Fig. 5 (top). The average temperatures over the eastern half of the country exhibit a dominant north–south latitudinal contrast, while influenced mostly by the mountain–desert configuration over the western half. The central states (i.e., Dakotas, Nebraska, Kansas, Oklahoma, and Texas) appear warmer than their neighboring states. Figure 5 (bottom) shows the temporal variance of monthly mean surface air temperature. Larger variance is found over the central states. The shaded area is a region characterized by strong positive skewness (greater than 0.3). Relatively brief episodes of significant above-normal temperatures are interspersed with more extensive periods of slightly below normal temperatures over the Mississippi River basin.

TABLE 2. Same as Table 1 but for Bismarck (49°N, 101°W).

Month	Yr	T − A (°C)	Month	Yr	T − A (°C)
Jul	1936	7.0	Jul	1915	−4.6
Jun	1933	5.0	Aug	1977	−3.7
Jun	1921	3.9	Jun	1945	−3.4
Aug	1937	3.8	Jul	1891	−3.3
Jun	1956	3.3	Jun	1915	−3.3
Jun	1931	3.0	Jun	1902	−3.3
Aug	1969	2.9	Aug	1974	−3.2
Aug	1961	2.8	Jul	1904	−3.0
Jun	1936	2.8	Jun	1951	−2.9
Jul	1937	2.8	Aug	1911	−2.8
Jun	1961	2.7	Jun	1916	−2.8
Jun	1919	2.7	Jun	1892	−2.8
Jun	1911	2.7	Jun	1928	−2.7
Jun	1910	2.6	Jun	1895	−2.7
Jul	1957	2.5	Jun	1969	−2.6

Positive skewness with a third-moment coefficient greater than 0.6 is observed over much of Illinois. The skewness for Kansas City is 0.5. The positive skewness

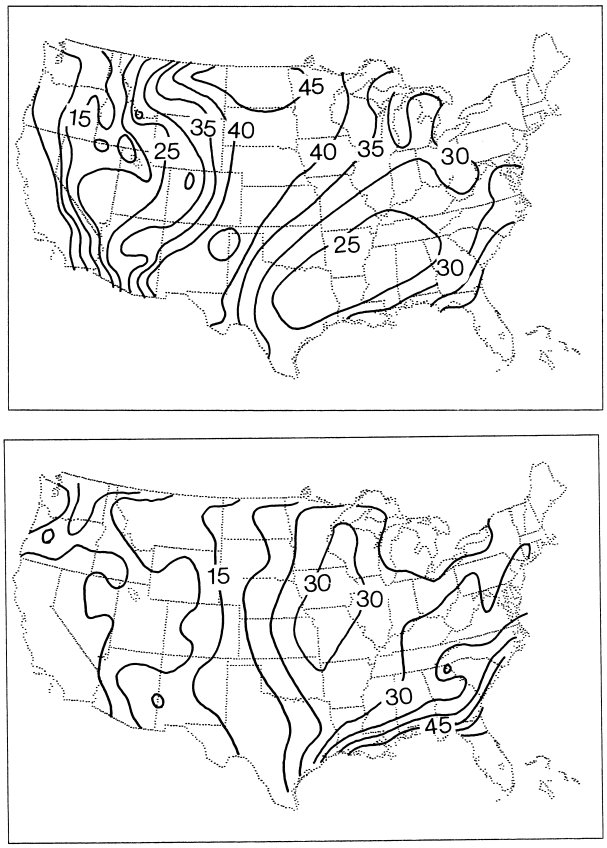

FIG. 6. (top) Fraction of rainfall falling during summer for same 156 month record as noted in Fig. 5; contour interval is 5%. (bottom) Climatological mean of summer monthly total precipitation for same period; contour interval is 5 cm.

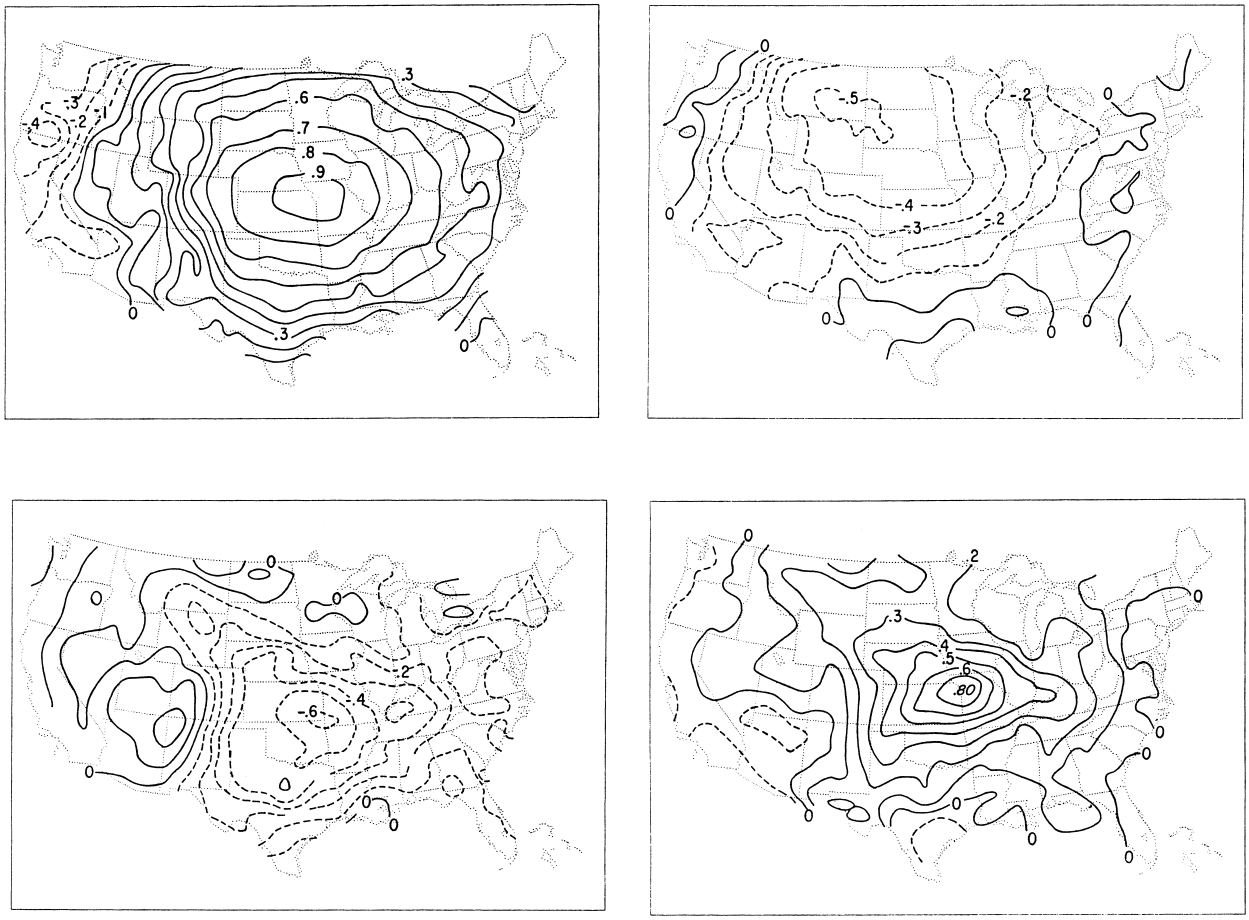

FIG. 7. (top) Correlation between monthly mean surface air temperature anomalies at Kansas City and those at every climate division; contour interval is 0.1. (bottom) Cross correlation between monthly mean surface air temperature anomalies at Kansas City and monthly total precipitation anomalies at every climate division; contour interval is 0.1. Record is based on 150 summer months from the 1931–80 period (50 yr).

FIG. 8. (top) Cross correlation between monthly total precipitation anomalies at Kansas City and monthly mean surface air temperatures at every climate division; contour interval is 0.1. (bottom) Cross correlation between monthly total precipitation anomalies at Kansas City and monthly total precipitation anomalies at every climate division; contour interval is 0.1. Record is based on same 150 months noted in Fig. 7.

of temperature anomalies at Bismarck is smaller than at Kansas City. Tables 1 and 2 indicate the 15 hottest and coolest months at Kansas City and Bismarck, respectively. The positive skewness at Kansas City can be attributed to the relatively larger positive anomalies of the first 15 hottest months contrasted to the negative anomalies of the 15 coolest months; the smaller skewness at Bismarck stems from only the four most extreme pairs of months contributing significantly. The characteristic temperature fluctuations of these two stations are different in that more nonsymmetry in temperature fluctuation is evident over Kansas City.

The mean summer seasonal rainfall, shown in the lower panel of Fig. 6, is between 15 and 30 cm everywhere in the United States east of the Rocky Mountains except along the south Atlantic and Gulf Coasts. Mean monthly rainfall during summer decreases sharply west of 100°W across the Great Plains. Figure 6 (top) shows that the 3-month summer season typically accounts for 40% of the annual average precipitation over the Great Plains. Moreover, the variability of summer monthly rainfall is large.

Negative correlations between temperature and precipitation were reported by Madden and Williams (1978) who analyzed seasonal mean data for 98 North American and European stations. These correlations were also evident on a monthly scale over the central and southern U.S. Great Plains during summer (Karl and Quayle 1981). CW87 confirmed these findings with the relationship being strongest over the Great Plains. For example, correlations stronger than -0.5 were found over much of the southern Great Plains (as shown in CW87's Fig. 2). Such correlations underlie the coupling between high surface air temperature and prolonged deficit rainfall concomitant with droughts, in which the severity and spatial pattern arise from the coupling.

CW87 quantified drought severity based on anomalies

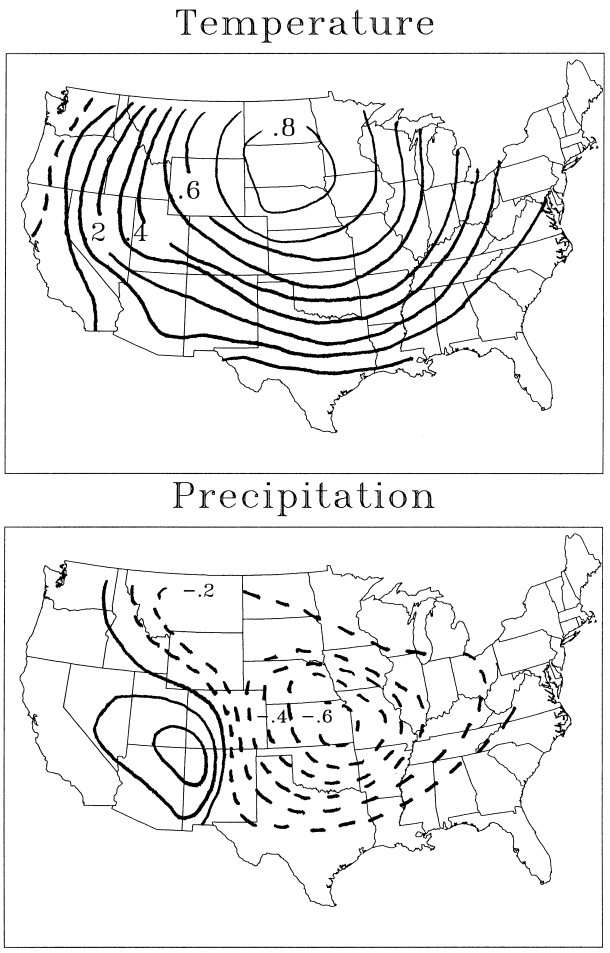

FIG. 9. Coupled mode of drought pattern for (top) temperature and (bottom) precipitation; contour interval is 0.1 for both panels. Pattern is derived from time series of climate divisional summer monthly mean surface air temperatures and total precipitation anomalies for 1895–1996 (102 yr).

of monthly mean surface air temperatures at Kansas City. Correlated occurrences of high surface air temperatures and deficit rainfall contributed to the success of their approach. The spatial coherence between either temperature or precipitation anomalies at Kansas City and those at every climate division during the 1931–80 period are shown in Fig. 7 (top) and Fig. 8 (bottom), respectively. Cross correlations between monthly mean surface air temperature (precipitation) anomalies at Kansas City and monthly precipitation (temperature) anomalies at every climate division are shown in Fig. 7 (bottom) [Fig. 8 (top)]. Results show that precipitation anomalies are closely linked to temperature anomalies at Kansas City and Bismarck. Section 5 examines this relationship for drought persistence.

b. Combined orthogonal rotated principal component analysis (CORPCA)

The above analysis indicates that the evolution of drought can be extracted from time series of monthly mean surface air temperatures and precipitation anomalies. However, any scheme to do so must isolate the coupled oscillation. Bretherton et al. (1992) discussed four analysis approaches for extracting a coupled mode of two variables. They are 1) single field principal component, 2) direct singular value decomposition, 3) canonical correlation, and 4) combined principal component.

Wallace et al. (1992) applied these techniques to identify the dominant coupled modes of wintertime sea surface temperatures and 500-mb height anomalies. Their results indicate that patterns derived from direct singular value decomposition and combined principal component analysis are similar. Here, we use CORPCA to isolate the drought pattern and its associated time series.

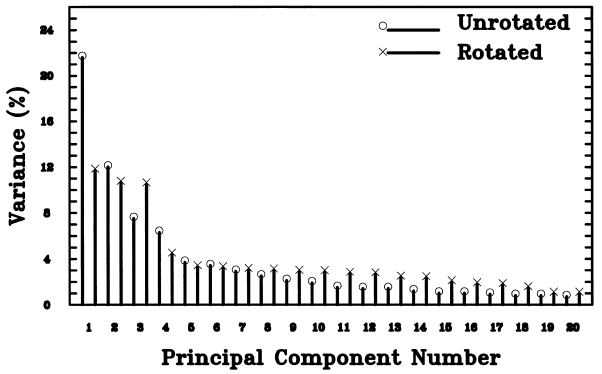

FIG. 10. Percentages of variance explained by first 20 unrotated (marked with Os) and rotated (marked with Xs) principal components derived from time series of climate divisional summer monthly mean surface air temperatures and total precipitation anomalies for same period indicated in Fig. 9.

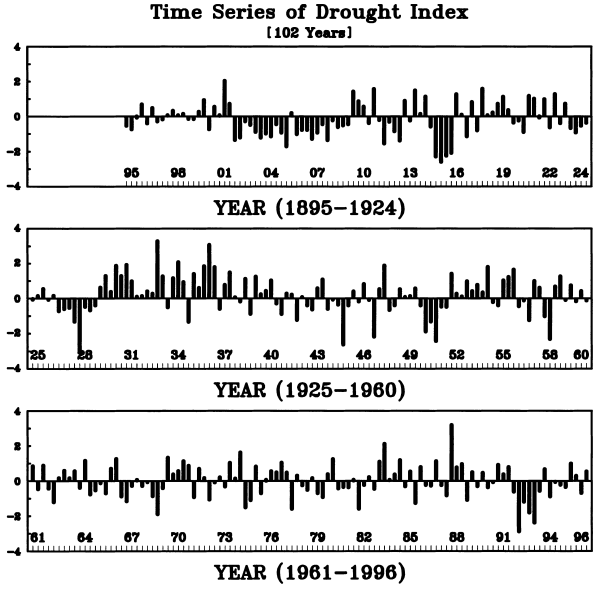

FIG. 11. Drought index indicating first orthogonal rotated principal component associated with drought pattern for 306 summer months for 1895–1996 period (102 yr).

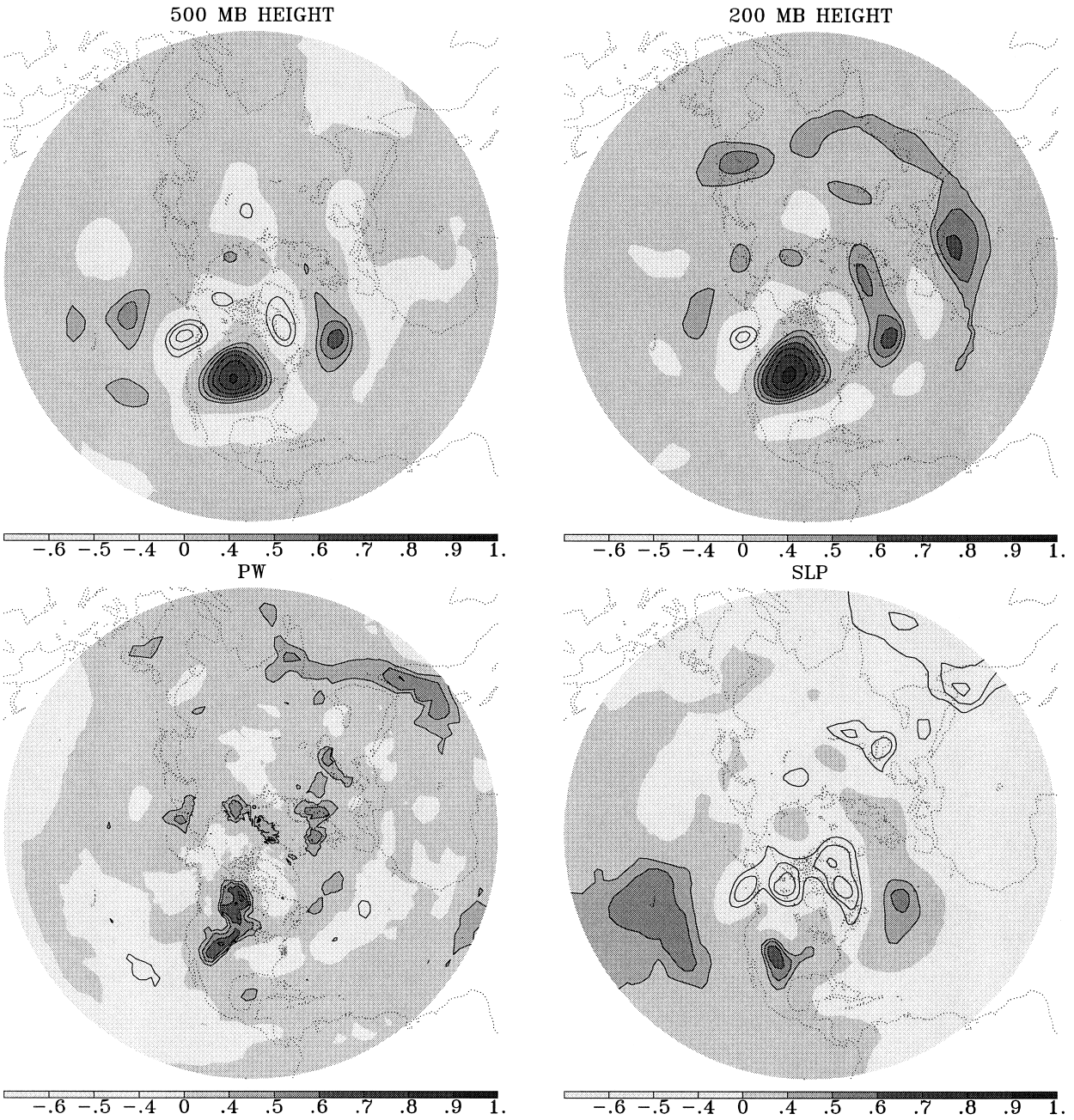

FIG. 12. Correlations between drought index and (top left) 500-mb height, (bottom left) total precipitable water, (top right) 200-mb height and (bottom right) sea level pressure. Record based on 39 summer months during the 1982–94 period (13 yr).

Lorenz (1956) pointed out that principal component analysis (PCA) can be extended to include two or more meteorological variables. In an application of PCA to a multifield composed of temperature, precipitation, and SLP, Kutzbach (1967) showed the internal consistency of these fields. Such an analysis approach is useful in identifying drought patterns.

The complexity of patterns obtained from PCA can be further simplified by linearly transforming the initial solution to an alternative solution. Here we use the Varimax rotation (Horel 1981), which increases the discrimination among the eigenvectors and makes the leading modes easier to interpret. The linear transform of the initial principal components utilizing the Varimax method is often referred to as orthogonal rotated principal component analysis. A reasonable approach to this simplification process is based on finding the maximum inequality in the distribution of variance among the sets of principal components. In other words, the transformation desired is one that will tend to further strengthen

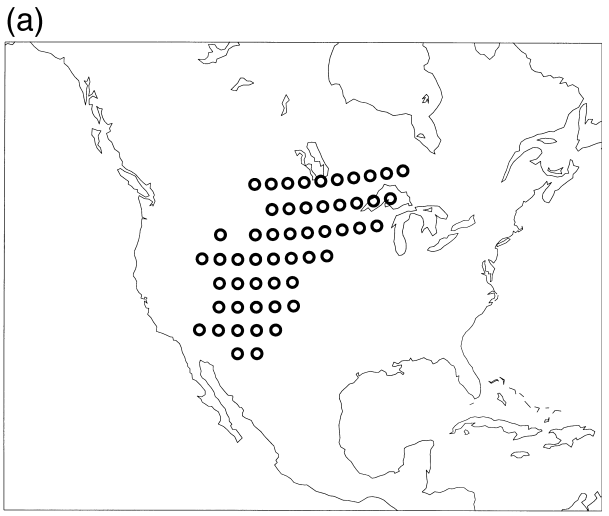

FIG. 13. (a) Circles show 52 NCEP grid points over east of Rocky Mountains, situated within shaded area over continental United States in PW anomaly map (Fig. 12 bottom left). (b) (top) Time series of PW averaged from 52 NCEP grid points over east of Rocky Mountains, situated within shaded area over continental United States in PW anomaly map as shown in Fig. 13a. (bottom) PW anomaly for Jun 1988, based on 13 Jun average from 1982 to 1994.

the strong correlations and to dilute the weak ones for each component of the original factor matrix. The mathematical approach maximizes the inequalities among the squares of the eigenvectors of the individual variables. More specific, the variance of the distribution of squared correlation coefficients between the rotated principal component and each of the original time series is maximized by an orthogonal transformation.

We apply this scheme to a hybrid field composed of normalized temperature and precipitation anomalies. Means and standard deviations were calculated for each of the months and for each of the variables. Anomalies from means are divided by the temporal standard deviation to from the normalized fields. CORPCA generates four types of results: 1) rotated time series referred to as rotated principal components, 2) amounts of variance explained by rotated principal components, 3) spatial patterns associated with rotated principal components referred to as rotated eigenvectors, and 4) correlations between unrotated and rotated principal components. The rotated eigenvectors reveal the dominant spatial patterns embedded in the dataset. The rotated principal components contain the amplitudes of the oscillation and their time evolution. The variances describe how much variation of the dataset can be attributed to each spatial and temporal mode.

c. Drought pattern and its time evolution over the United States Great Plains

We utilize CORPCA on the time series of climate divisional monthly mean surface air temperatures and precipitation anomalies for 306 summer months (1895–1996). Correlated occurrence of high (low) surface air temperature and deficit (excess) rainfall over the Great Plains emerges as the dominant pattern (Fig. 9). The center of maximum amplitude in precipitation fluctuation (Fig. 9: bottom) is found near Kansas City, while that of temperature is found over South Dakota (Fig. 9: top). Kansas City exhibits the higher correlation in this pattern—both temperature and precipitation correlation values are around ± 0.6. The salient feature of this drought pattern is the internal consistency between temperature and precipitation.

Similar patterns were apparent in an earlier analysis (Chang 1986) for a shorter period (June–August 1931–82). The stability of this pattern was tested by dividing the 52-yr period into even and odd years. The results from all three groups are similar to those shown in Fig. 9. The effect of the number of principal components retained for rotation was also examined. Here, we use the Guttman lower bound criterion, which includes principal components contributing more than 1% to the total variance (Guttman 1954). The first 20 principal components in this analysis contribute more than one unit of total variance and are retained for rotation. The sensitivity of changing the remaining number of principal components is also tested. Experiments indicate that similar patterns can be transformed from slightly less than 20 or slightly more than 20 principal components. The robustness of the drought pattern is evident in the analysis. Figure 10 shows percentages of variance explained by the first 20 unrotated and rotated components. The drought pattern explains 12% of the total variance.

The first principal component (Fig. 11) is used as an index to quantify the severity of drought over the Great Plains during the period of 1895–1996. It is different from PDSI in the sense that it is a single number to quantify the severity of drought over the Great Plains, while PDSI is point by point. It is more objective than using direct temperature anomalies at Kansas City as in CW87. Large positive (negative) principal components represent months with deficit (excess) rainfall and high (low) surface air temperature over the Great Plains. The twelve severest drought months (in order) during this period are June 1933, June 1988, July 1936, August 1983, July 1934, July 1901, June 1931, August 1947, July 1930, June 1936, July 1954, and August 1936. Nine out of these 12 months are in the 1930s and 1980s. The index also reveals the most recent flood prone months, that is, July 1992 and July 1993. In comparison with the Kansas City surface air temperature anomalies (see Fig. 3), the drought index successfully quantifies drought severity, as verified by a correlation coefficient of 0.735 for the 258 months (1895–1980).

5. Dynamical and hydrological characteristics of droughts

a. Large-scale features

NCEP reanalysis of SLPs, 500- and 200-mb geopotential heights, and PWs are now used to analyze dy-

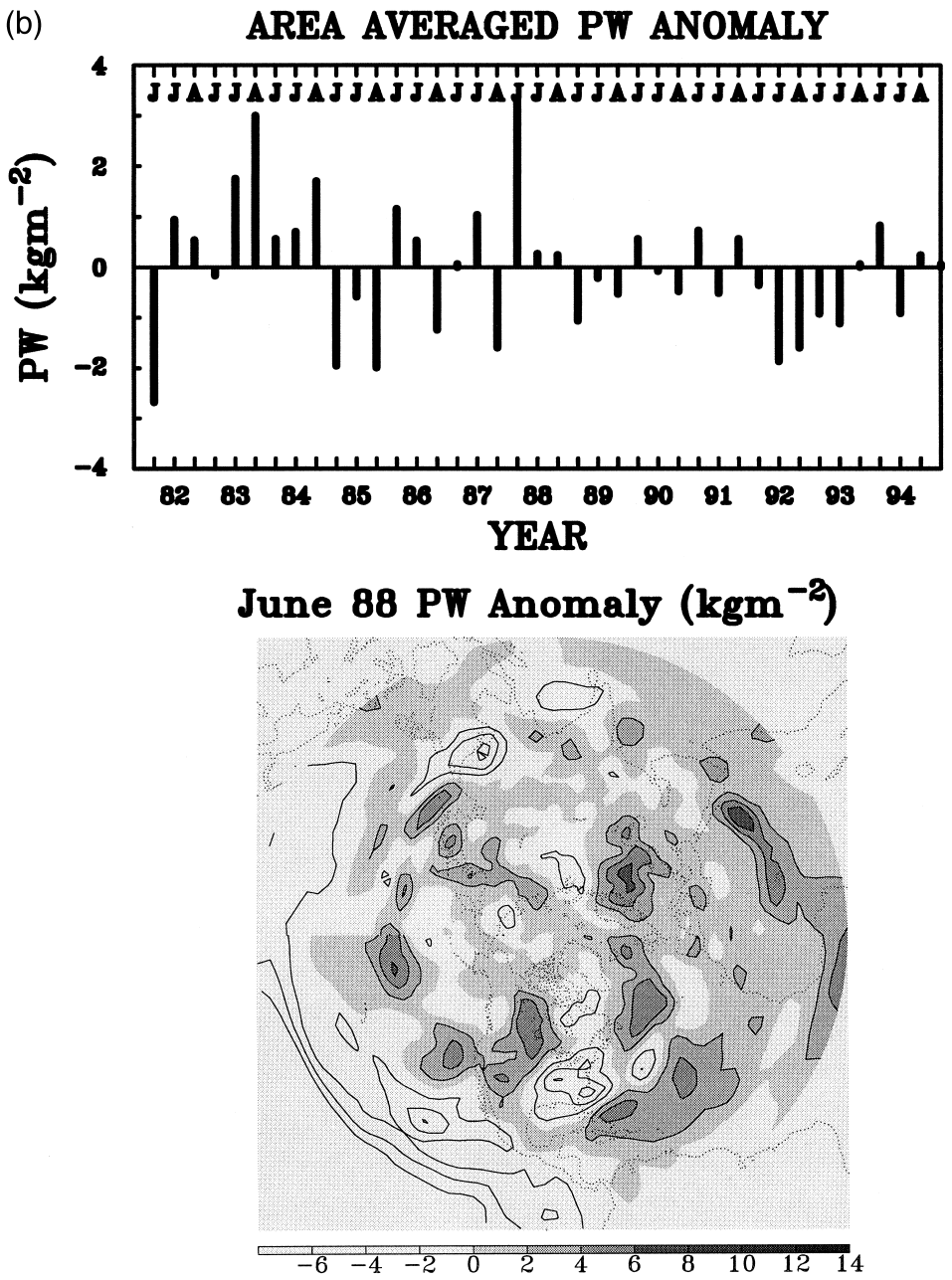

FIG. 13. (*Continued*)

namical processes and their relationship to the maintenance of drought. These data have been archived on the first released NCEP reanalysis product, that is, a CD-ROM published with the 1996 March issue of the *Bulletin of the American Meteorological Society* (Kalnay et al. 1996). Precipitable water is the integrated moisture content for unit cross section extending from the earth's surface to the atmosphere's top, given as the integral $\mathrm{PW} = (1/g) \int q(p)\, dp$, where $q(p)$ is the vertical profile of specific humidity, and PW is expressed in units of mass per area (or units of length after division by water density).

The drought index has been temporally correlated with PW, both 500- and 200-mb geopotential heights, and SLPs at every grid point over the Northern Hemisphere to produce large-scale interrelationship maps. The data being used are from the same 39 months used in the teleconnectivity calculations. Figure 12 shows the 500-mb geopotential height (top left), PW (lower left), 200-mb geopotential height (top right), and SLP (lower right) maps. Shaded areas indicate correlation values are positive; contour lines begin at ± 0.4 with an interval of 0.1.

A wavelike pattern appears on the 500-mb geopoten-

tial height correlation map throughout the Pacific–North America–Atlantic sector. The positive centers are situated over the North Pacific just north of the Hawaiian Islands, North America centered over the Dakotas, and the North Atlantic just west of the British Isles; the negative centers are situated in the southeastern Gulf of Alaska and Davis Strait. The most prominent feature is the strong anticyclone over central North America. Note both centers of maximum temperature fluctuation (Fig. 9) and strongest 500-mb geopotential height correlation (Fig. 12) are over the Dakotas. The locations of primary centers are similar to those in CW87 based on Kansas City temperature anomalies and NMC analyses.

Major features in the 200-mb geopotential height correlation map are similar to those in the 500-mb map; however, the prominent positive correlation region over central North America appears larger. The center is at (42.5°N, 102.5°W) just west of that in the 500-mb map. Below-normal 200-mb heights are also found in the southeastern Gulf of Alaska, with their strengths slightly weaker than those at the 500-mb level. The center over the Atlantic is extended northeast to the Norwegian Sea. Large-scale features appear over the Eurasian–African–Atlantic sector on the 200-mb geopotential height map. Positive centers are found over the Sahara and East China Sea.

The main features of the corresponding SLP correlation map (Fig. 12: bottom) are similar to those of the SLP teleconnectivity map (Fig. 2). Positive correlations are found over three regions centered at (20°N, 140°W) in the North Pacific, (35°N, 107.5°W) in New Mexico, and (40°N, 37.5°W) in the North Atlantic. Regions with opposite polarity are found over the higher latitudes extending from the Gulf of Alaska, through Canada, the Davis Strait, and on to Greenland. This indicates that droughts occur concurrently with all of the teleconnection patterns. Negative correlations are also found over a region from Somalia to the southern tip of India.

In summary, above-normal SLPs over New Mexico, the North Atlantic, and the subtropical Pacific along with below-normal SLPs over the Gulf of Alaska eastward to Greenland are present during Great Plains drought occurrences. Features over North America are different from those identified in CW87 based on NCEP analyses and Kansas City surface air temperature anomalies (see their Fig. 3). This analysis indicates that above-normal SLPs over New Mexico are associated with droughts over the Great Plains, while CW87 found a deeper-than-normal low over the Rocky Mountains during drought episodes. Furthermore, the agreement between the drought-SLP pattern in Fig. 12 over North America with the Great Basin heat island regime identified by Tang and Reiter (1984) suggests monsoonal fluctuations are linked to Great Plains drought.

b. Regional scale features

Large variations of water vapor content over the Rocky Mountains create the maximum in the PW correlation map (see Fig. 12: bottom). A range of correlation from 0.4 to 0.7 is found over a relatively narrow strip from New Mexico and Arizona (~113°–104°W), extending to Utah and Colorado, Wyoming and Nebraska, and into the Dakotas and Minnesota (~106°–85°W). This strip contains the maximum PWs over the Great Plains during drought months. It is related to how moisture transport from the Gulf of California into the Great Plains across the southwestern corridor (see Rasmusson 1968) is prevented from reaching the Mississippi valley. This comes about by the low-level warm southerly flow on the west side of the westward displaced Bermuda high enhancing the preexisting north-to-south temperature gradient, and thus stimulating a zonal wind reversal across the central Great Plains through the thermal wind relationship (this will be further discussed below in conjunction with Fig. 15). Large variations in PWs also appear over the region from eastern Africa eastward to India.

Figure 13a shows the 52 NCEP grid points situated over this maximum PW strip within the U.S. continent. Figure 13b (top) shows the time series of area-averaged PW anomalies over these 52 NCEP grid points during the 1982–94 period. Largest positive anomalies are found during June 1988 and August 1983, with negative anomalies during July 1992 and 1993. The Mississippi River basin exhibits below normal PWs (i.e., negative correlations), although correlations do not fall below −0.4. Below normal PWs are found over the subtropical oceans accompanying above-normal SLPs during droughts. These features are evident in the June 1988 PW anomaly field (Fig. 13b bottom).

Low-level warm advection (resulting in elevated surface temperatures) and large-scale subsidence (resulting in elevated midtropospheric temperature) during drought months combine to produce warm temperatures throughout the tropopause. This is evident from a comparison of thicknesses of the 1000- to 500-mb layer during June 1988 (Fig. 14: bottom) and the averages from 13 Junes from 1982 to 1994 (Fig. 14: top). The thermal trough shifts east during June 1988. Thus the pressure gradient force at midtroposphere levels is directed away from the Dakotas above an eastward-positioned shallow heat low (east of 100°W) that results from strong surface heating. Note that the positive SLP correlations over New Mexico (see Fig. 12) suggest a relative low SLP region over South Dakota. Direct evidence for the heat low is found in the left panels of Fig. 16a showing vertical velocity cross sections; this feature is akin to the Great Basin heat lows described in Tang and Reiter (1984). Higher-than-normal thicknesses (~5760 versus ~5720 m) around the Dakotas appear during June 1988. This high-temperature pattern with lower temperatures over Texas during June 1988 reduces the westerly wind strength. In fact, easterlies appear at the 600-mb level south of Kansas City (see Fig. 15) as discussed earlier.

Zonal cross sections for vertical velocities over a lon-

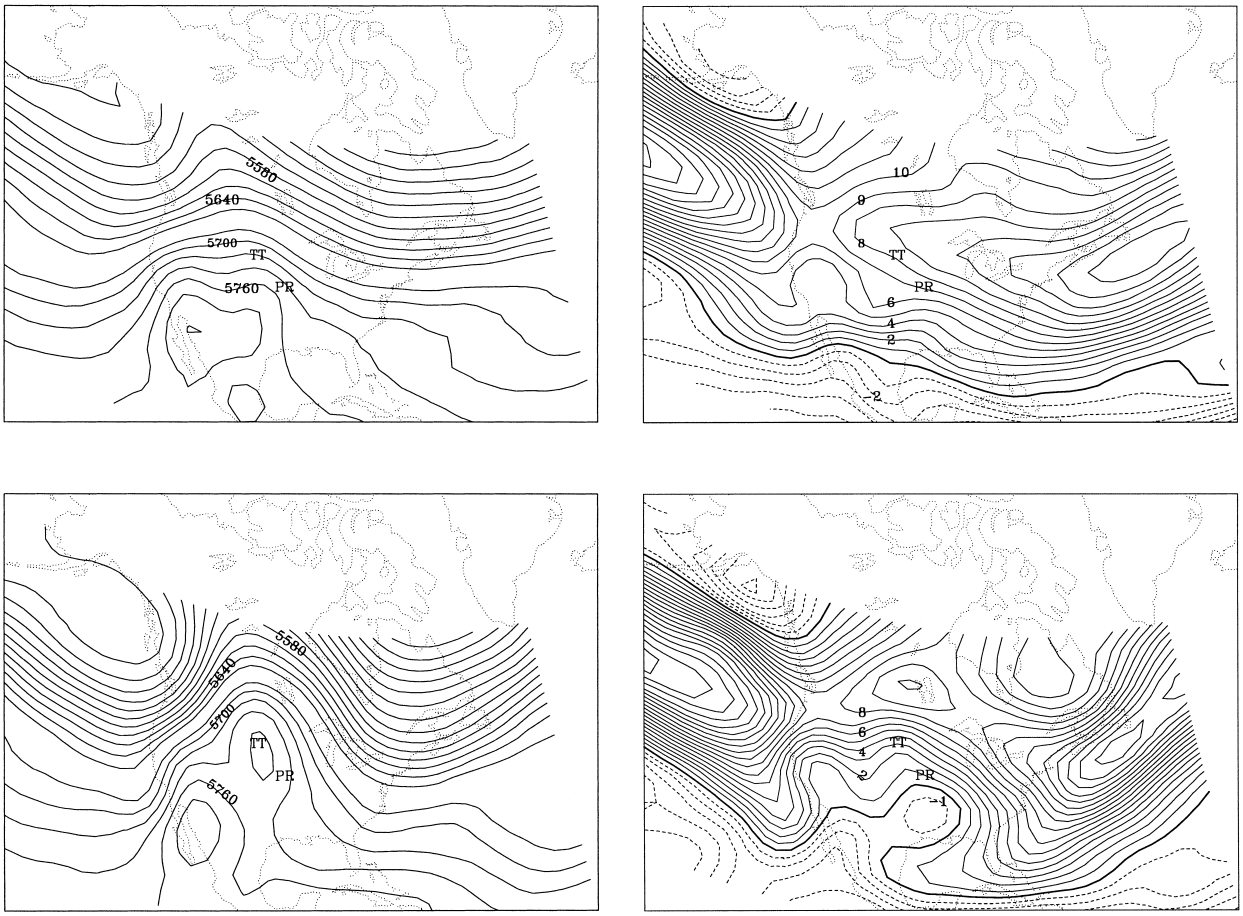

FIG. 14. (top) 1000- to 500-mb thickness (m) composite for Jun throughout 1982–94 period (13 yr). (bottom) Thickness field for Jun 1988. Symbols TT and PR indicate center of maximum amplitude in temperature and rain fluctuations, respectively.

FIG. 15. (top) Zonal wind composite at 600 mb (m s^{-1}) for Jun throughout 1982–94 period (13 yr). (bottom) Winds for Jun 1988. Symbols TT and PR indicate center of maximum amplitude in temperature and rain fluctuations, respectively.

gitudinal sector from 110° to 82.5°W, at latitudes 45°N, 42.5°N, 40°N, and 37.5°N are shown in Figs. 16a,b. Rising motion up to 600 mb and sinking motion from 250 to 500 mb are found over the thermal heat low situated over eastern South Dakota (~45°N, 97.5°W) during June 1988. Sinking motion over the Kansas City area (~40°N, 95°W) during the same month is stronger than the climatological mean based on the 1982–94 June average (Fig. 16b). Surface air temperatures warm, relative humidities drop, and sinking motion seeks to balance the enhanced radiative cooling caused by increased atmospheric transmittances in both solar and infrared spectrums around Kansas City. Hence, following Charney et al.'s (1977) suggestion, net tropospheric cooling plays an important role in the maintenance of drought over the U.S. Great Plains.

Figure 17 shows the June 1988 temperature anomaly profiles for grid points (~45°N, 97.5°W) and (~40°N, 95°W). Both locations show positive anomalies up to 250 mb. Below normal temperature anomalies are observed at the 200- and 150-mb levels with about equal strengths at the lower level. Temperature anomalies over South Dakota are larger than over Kansas City. Positive temperature anomalies are decreasing from 850 to 400 mb over South Dakota while those over Kansas City are increasing from 850 to 600 mb.

c. *Drought maintenance*

A number of factors are crucial to the maintenance of the U.S. Great Plains droughts. These factors include enhanced moisture transport from the Gulf of California, warm surface air flow from the southwest United States into the Dakotas, elevated PWs east of the Rocky Mountains, low precipitation around the Kansas City area, a thermal heat low over South Dakota, anomalous zonal winds, and vertical velocity. The schematic diagram shown in Fig. 18 is used to interpret the linkage between the above factors including the vertical shear of the geostrophic wind ($\mathbf{V}_g$). The geostrophic wind for an equivalent barotropic or generally baroclinic atmosphere for any two pressure levels p_1 and p_2, at a given

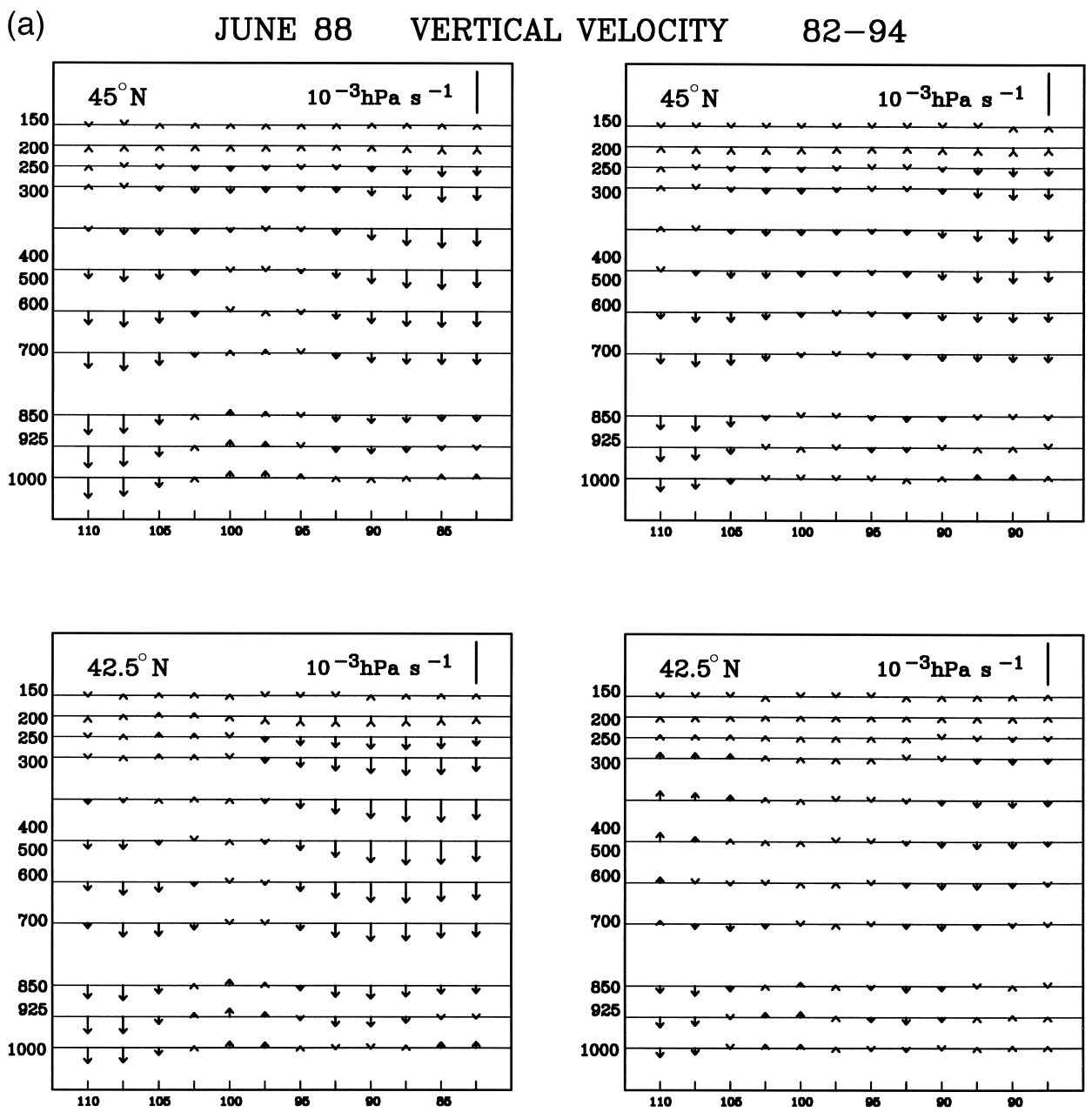

FIG. 16. (a) (left) zonal cross section of vertical velocities (reference scalar: 10^{-3} hPa s^{-1}) for Jun 1988 at 45° and 42.5°N over longitudinal section from 110° to 82.5°W. (right) Cross sections for 13 Jun average (1982–94). (b) Same as Fig. 16a, but for 40° and 37.5°N.

Coriolis parameter f, can be expressed as $\mathbf{V}_g(p_2) - \mathbf{V}_g(p_1) \simeq (-R/f)(dT_m/dn)\ \ln(p_1 - p_2)\mathbf{k}$, where R and T_m are the universal gas constant and layer mean temperature, respectively, n denotes a scalar distance along the vertically projected temperature gradient, $\mathbf{k}$ is the appropriate directional unit vector, and the thickness of a layer (e.g., 1000–500 mb) is proportional to the layer temperature.

Figure 18 shows how the thickness structure changes from normal conditions (top schematic) to drought conditions (lower schematic) with the associated temperature gradient change causing the geostrophic winds to decrease with height and to reverse during droughts when the temperature gradient reverses. This is enhanced by warm surface flow behind the westward displaced Bermuda high into the Dakotas. Given enhanced moisture transport from the Gulf of California, shallow rising motion over the local thermal heat low and southward midlevel returning flow in conjunction with the easterlies south of Kansas City and the associated convergence maintain elevated PWs east of the Rockies while reducing moisture convergence into the Missis-

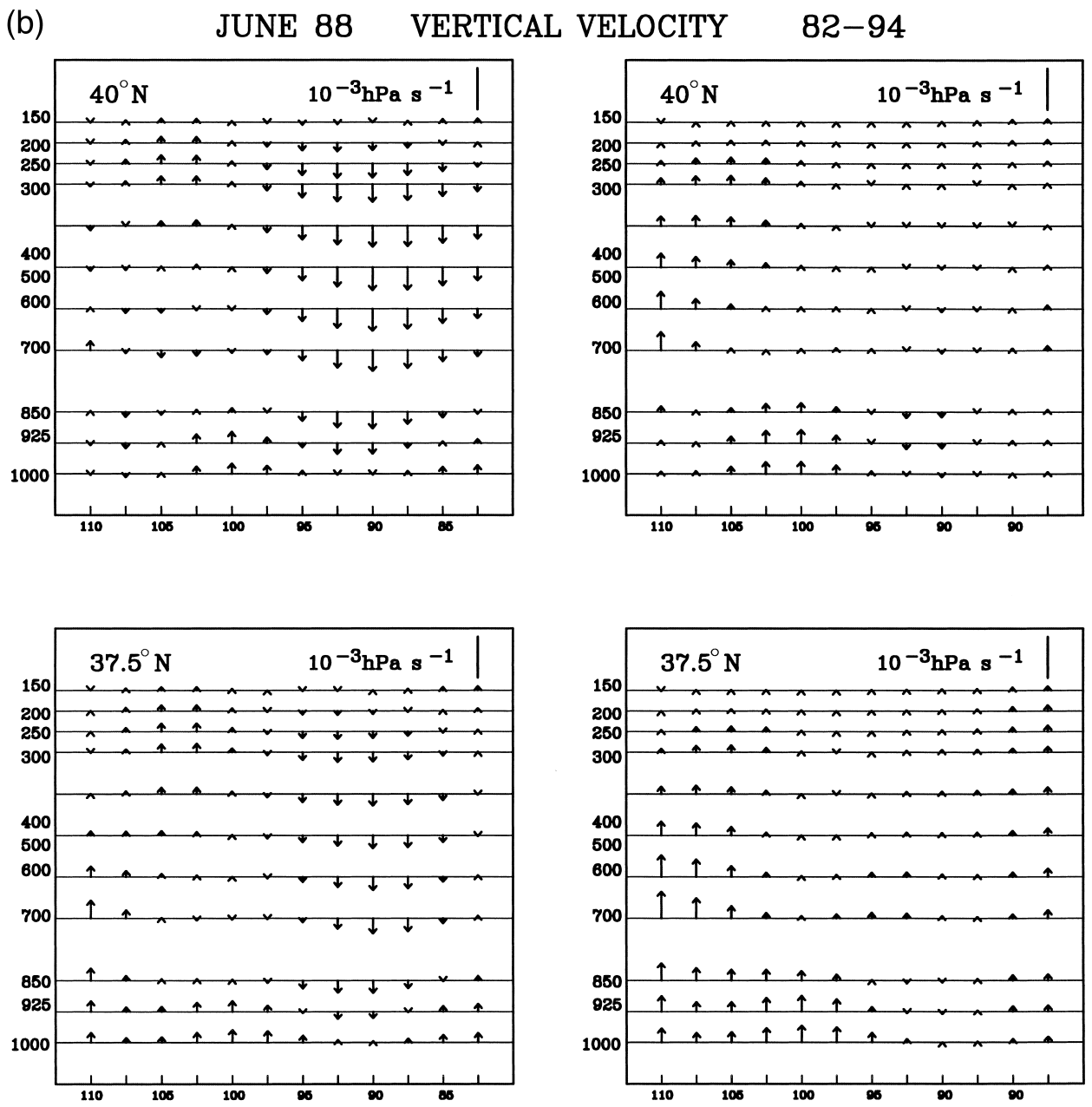

FIG. 16. (*Continued*)

sippi valley. This local feedback mechanism helps to amplify the maximum amplitude of temperature and precipitation fluctuations and, in turn, radiatively driven enhanced sinking and the strength of the initial middle-upper level circulation anomaly over central North America as evident in the strongest feature in the Fig. 12 (top) correlation maps.

d. Hydrological considerations

Hydrological conditions are further examined by using monthly surface observations over Kansas City and Bismarck, near the centers of the drought. Statistics observed at Kansas City along with the drought index for the 20 severest drought- and flood-prone months are listed in Tables 3 and 4. High surface air temperature and deficit rainfall are observed for all drought months given in Table 3—except August 1947. The temperature anomaly for August 1947 is 4.4°C, with precipitation slightly above normal. The flood-prone months indicate low surface air temperatures and excess rainfall—except during both August 1911 and 1912.

Table 3 shows that droughts over the Great Plains generally exhibit negative surface relative humidity

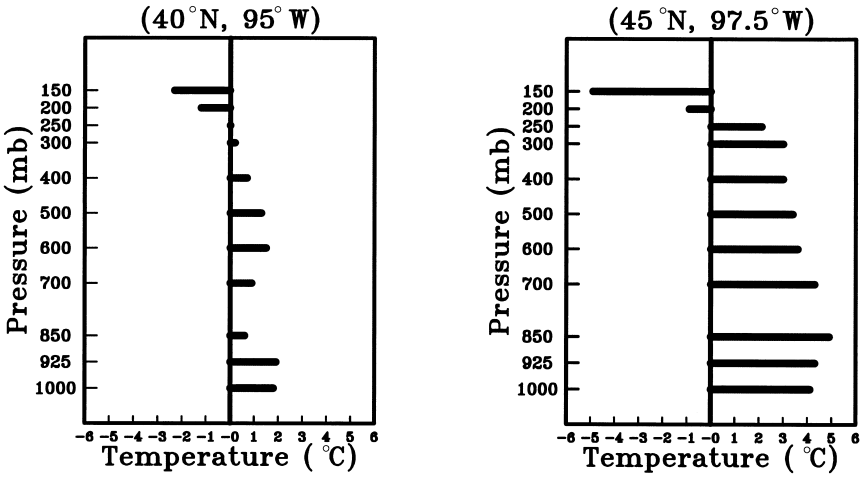

FIG. 17. Temperature anomaly profiles near Kansas City (40°N, 95°W) and Redfield, SD, (45°N, 97.5°W) for Jun 1988 using 13-yr Jun average (1982–94) as normal.

anomalies, with larger-than-normal monthly mean daily temperature ranges. These statistics are consistent with the process of radiatively driven enhanced sinking motion over the Kansas City area, an important characteristic of summertime droughts. More than one-half of the drought months have negative relative humidity anomalies at least 10% below normal, while only four flood-prone months have positive relative humidity anomalies greater than 10% above normal. Together with the positive skewness shown in Fig. 5 and Table 1, nonsymmetries in the summertime climate fluctuations at Kansas City are evident.

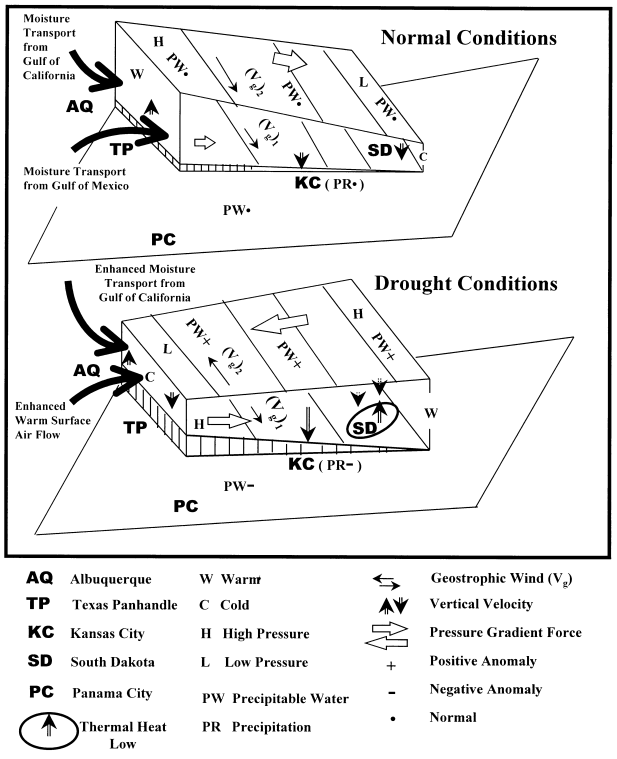

FIG. 18. Schematic diagram indicating zonal wind changes in response to thermal heat low conditions over SD during drought period [(top) normal month; (bottom) drought month].

The statistics at Bismarck are presented in Tables 5 and 6. Temperature anomalies for all drought- (flood-) prone months are positive (negative). As shown in Fig. 9, precipitation at Bismarck is only marginally correlated with drought index. Given that low-level rising motion is observed around Bismarck during drought months (Fig. 16a), the lower correlation in precipitation is not a surprise. In general, the drought- (flood-) prone months are also characterized by below- (above-) normal relative humidities.

Charney et al. (1977) defined the western Great Plains as a region over 32°–48°N and 107.5°–97.5°W, with the Mississippi valley extending from the same latitude belt and from 92.5° to 82.5°W in longitude. In a modeling study of drought onset and maintenance they performed a simulation with increased albedo over the western Great Plains and another with increased albedo over the western Great Plains and Mississippi valley. Our results indicate that the maximum amplitude in temperature of the drought pattern is located over South Dakota, while that of precipitation is located over the Mississippi valley. On the assumption albedo is directly correspondent to precipitation/drought anomalies, Charney et al.'s manipulation of anomalies for the albedo impact simulations are not consistent with anomalies found in the data for the last 100 yr.

Numerical simulations of the influence of surface albedo and soil moisture anomalies on the summer circulation were also published by Sud and Fennessy (1982, 1984). They increased surface albedo and decreased soil moisture over the western Great Plains. Below-normal surface temperatures and unchanged precipitation were obtained for their anomalously high surface albedo simulation while above-normal surface tem-

TABLE 3. Monthly statistics observed at Kansas City (39°N, 95°W) for 20 severest drought-prone months over central Great Plains during period 1895–1996, ranked on basis of drought index shown in Fig. 11. Monthly statistical parameters are maximum temperature (Max), minimum temperature (Min), daily temperature range (Range), temperature anomaly (T − A), total precipitation anomaly (P − A), dew point anomaly (T_d − A), and relative humidity anomaly (RH − A).

Rank	Year	Month	Index	Max (°C)	Min (°C)	Range (°C)	T − A (°C)	P − A (cm)	T_d − A (°C)	RH − A (%)
1	1933	6	−3.29	33.5	21.9	11.6	3.9	−6.5	−2.2	−0.4
2	1988	6	−3.19							
3	1936	7	−3.06	38.5	23.5	15.0	4.4	−8.5	−3.0	−20.0
4	1983	8	−2.12							
5	1934	7	−2.08	38.8	23.8	15.0	4.8	−3.6	−3.0	−21.0
6	1901	7	−2.02	36.8	24.4	12.4	4.0	−2.4	−1.9	−17.0
7	1931	6	−1.91	31.7	21.0	10.7	2.8	−8.2	0.5	−8.0
8	1947	8	−1.88	36.0	24.2	11.8	4.4	1.1	2.0	−7.0
9	1930	7	−1.87	33.9	22.2	11.7	1.7	−5.9	−3.6	−16.0
10	1936	6	−1.84	33.3	18.3	15.0	2.0	−10.7	−3.3	−17.0
11	1954	7	−1.79	37.0	24.2	12.8	4.0	−7.0	−1.3	−16.0
12	1936	8	−1.78	37.9	23.3	14.6	4.9	−9.3	−1.9	−18.0
13	1956	6	−1.64	30.1	20.0	10.1	1.7	−2.9	0.5	−5.1
14	1974	7	−1.63	35.0	20.6	14.4	1.2	−6.5	−2.5	−13.8
15	1918	6	−1.57	32.2	21.1	11.1	2.9	−8.2	−1.1	−10.0
16	1911	6	−1.57	32.7	21.6	11.1	3.4	−11.2	−1.7	−16.0
17	1937	8	−1.48	34.6	22.9	11.7	3.1	−4.2	1.5	−2.0
18	1913	8	−1.48	35.7	23.5	12.2	4.0	−7.6	−3.5	−22.0
19	1952	6	−1.41	34.6	22.8	11.8	5.0	−2.7	2.2	−8.0
20	1909	8	−1.41	37.2	22.2	10.0	1.3	−8.9	0.3	−4.0

perature and unchanged precipitation were obtained for their low–soil moisture simulations. Hence, their results suggested that the western Great Plains did not follow Charney's simple hypothesized biogeophysical feedback mechanism. However, in view of two conditions Sud and Fennessy employed in their simulations, 1) an initial condition of 15 June 1979 that did not trigger an anomalous atmospheric circulation for drought conditions and 2) localized surface albedo and soil moisture anomalies covering the western Great Plains but excluding the Mississippi valley, such a contradiction might be expected. Their studies serve as evidence that there is a linkage between dynamical and hydrological processes for drought maintenance over the Great Plains, but it is important that the anomaly forcing be realistic.

6. Conclusions

Correlations between a drought index and geopotential heights indicate a teleconnection between Great Plains drought and climate fluctuations over other parts

TABLE 4. Same as Table 3, but for 20 severest flood-prone months.

Rank	Year	Month	Index	Max (°C)	Min (°C)	Range (°C)	T − A (°C)	P − A (cm)	T_d − A (°C)	RH − A (%)
1	1928	6	3.07	24.9	15.5	9.4	−3.6	1.8	−2.2	6.0
2	1992	7	2.88							
3	1945	6	2.62	25.0	16.1	8.9	−3.2	3.3	−1.7	6.0
4	1915	7	2.59	28.5	18.9	9.6	−2.9	7.6	−0.2	10.0
5	1951	6	2.42	25.9	15.9	10.0	−2.8	9.4	0.0	11.0
6	1993	7	2.38							
7	1958	7	2.32	29.4	20.6	8.8	−1.6	17.8	1.4	9.2
8	1915	6	2.29	25.6	16.7	8.9	−2.6	8.0	−0.6	9.0
9	1915	8	2.24	25.4	17.1	8.3	−4.5	1.4	−2.4	9.0
10	1947	6	2.17	28.3	17.8	10.5	−0.7	8.8	1.1	5.9
11	1916	6	2.08	26.1	16.7	9.4	−2.3	2.0	−1.7	2.0
12	1950	7	1.89	27.2	17.8	9.4	−4.1	15.8	2.0	14.0
13	1969	6	1.88	26.2	16.1	10.1	−2.5	14.8	−0.6	5.0
14	1993	6	1.80							
15	1905	7	1.70	28.0	19.1	8.9	−3.0	9.3	−0.8	8.0
16	1982	6	1.59							
17	1977	8	1.59	28.8	18.3	10.6	−0.4	10.3	2.0	14.7
18	1911	8	1.54	30.6	20.6	10.0	−0.1	−4.1	−1.3	−4.0
19	1974	8	1.50	28.3	17.2	11.1	−2.9	2.6	−0.8	9.0
20	1912	8	1.39	30.0	20.0	10.0	−0.6	−0.4	0.3	4.0

TABLE 5. Same as Table 3, but for Bismarck (49°N, 101°W).

Rank	Year	Month	Index	Max (°C)	Min (°C)	Range (°C)	T − A (°C)	P − A (cm)	T_d − A (°C)	RH − A (%)
1	1933	6	−3.29	30.1	15.7	14.4	5.0	−3.3	1.1	−11.0
2	1988	6	−3.19							
3	1936	7	−3.06	36.7	20.6	16.1	7.0	−5.3	−1.3	−22.0
4	1983	8	−2.12							
5	1934	7	−2.08	31.1	16.1	15.0	1.9	−3.1	−1.9	−11.0
6	1901	7	−2.02	28.8	16.6	12.2	1.3	2.7	3.1	7.0
7	1931	6	−1.91	27.8	14.4	13.3	3.0	−4.0	0.6	−7.0
8	1947	8	−1.88	30.6	15.6	15.0	2.3	−1.5	1.9	3.0
9	1930	7	−1.87	31.7	15.6	16.1	2.2	−0.7	−0.8	−8.0
10	1936	6	−1.84	28.3	13.3	15.0	2.8	−7.0	−3.3	−18.0
11	1954	7	−1.79	29.4	15.5	13.9	0.9	4.5	2.0	4.0
12	1936	8	−1.78	30.0	15.5	14.4	2.2	−2.8	−2.5	−11.0
13	1956	6	−1.64	28.9	13.9	15.0	3.3	−2.2	2.2	−4.0
14	1974	7	−1.63	32.2	14.4	17.8	1.6	−2.7	−0.8	−8.0
15	1918	6	−1.57	25.5	12.2	13.3	0.9	−6.7	−0.5	−6.0
16	1911	6	−1.57	27.2	13.9	13.3	2.7	−1.3	2.2	3.0
17	1937	8	−1.48	31.6	16.6	15.0	3.8	−1.5	−0.9	−13.0
18	1913	8	−1.48	30.0	13.9	16.1	1.4	−2.4	0.8	2.0
19	1952	6	−1.41	27.2	11.7	15.5	1.7	0.0	0.0	−3.0
20	1909	8	−1.41	29.4	14.4	15.0	1.5	7.8	3.6	9.0

of the Northern Hemisphere. Dynamical conditions, as described in NCEP reanalysis 500- and 200-mb geopotential heights, reveal a middle- and upper-troposphere wave train with positive centers over the North Pacific just north of the Hawaiian islands, North America centered around South Dakota, the North Atlantic just west of the British Isles; and negative centers in the southeastern Gulf of Alaska and Davis Strait. A seesawing in sea level pressure centered between New Mexico (above normal) and Gulf of Alaska (below normal) is present during drought months. Drought occurs in connection with virtually all sea level pressure teleconnection patterns. Above-normal sea level pressures over New Mexico, the North Atlantic, and the subtropical Pacific and below-normal sea level pressures over the Gulf of Alaska eastward to Canada, Davis Strait, and Greenland are thus linked to droughts over the Great Plains.

The prominent feature of a strong anticyclone over central North America during intense droughts highlights the land surface feedback mechanism. Focusing on North America, we transcribed the contours given in Fig. 12 with correlations stronger than 0.4 for 500-mb geopotential height, precipitable water, and sea level pressure into Fig. 19. These results show that the center of maximum temperature fluctuation of the drought lies at the 500-mb anticyclone anomaly center over South Dakota, while the center of maximum precipitation fluctuation lies over the Kansas City area.

Maximum precipitable water concentrations are confined to a strip of approximately 10° of longitude from New Mexico and Arizona (~113°–104°W), extending to Utah and Colorado, Wyoming and Nebraska, on into the Dakotas and Minnesota (~106°–85°W); see Fig. 13a. Multiple processes work together to maintain the maximum moisture concentrations east of the Rocky Mountains. Large-scale pressure anomalies enhance water vapor transports from the Gulf of California, while the north–south temperature gradient reversal and concomitant easterly zonal flow south of Kansas City produce the essential convergence mechanism against the eastern Rockies. The warm low-level southwesterly flow behind the westward displaced Bermuda high also serves to maintain the moist band by enhancing the positive temperature anomaly over South Dakota. Enhanced solar and infrared absorption processes also serve to build the mid- to upper-tropospheric warm anomaly and high pressure over South Dakota, which is a key element of a broad enhanced subsidence zone over the Great Plains essential for drought conditions.

The middle tropospheric easterlies over the central Great Plains cut off water vapor advection into the Mississippi valley including the Kansas City area. Enhanced subsidence over Kansas City then leads to further drying. Hydrological characteristics, as revealed in the monthly surface observations at Kansas City and Bismarck, explain why droughts over the Great Plains exhibit negative surface relative humidity anomalies (consistent with anomalous sinking motion), with larger-than-normal monthly mean daily temperature ranges.

The observational analysis provides evidence of linkage between Great Plains droughts and climate fluctuations over other parts of the Northern Hemisphere. Atmosphere–land surface feedbacks create a preferred spatial drought pattern, a thermal heat low over South Dakota with low precipitation around the Kansas City area. Vertical motions and relative humidities during severe droughts are consistent with the biogeophysical hypothesis, but a number of other factors are also at work. For example, elevated PWs east of the Rocky Mountains are important to drought maintenance because the hydrological–radiative–thermodynamical–dynamical cou-

TABLE 6. Same as Table 5, but for 20 severest flood-prone months.

Rank	Year	Month	Index	Max (°C)	Min (°C)	Range (°C)	T − A (°C)	P − A (cm)	T_d − A (°C)	RH − A (%)
1	1928	6	3.07	21.1	8.9	12.2	−2.7	4.0	−2.2	2.0
2	1992	7	2.88							
3	1945	6	2.62	20.6	8.3	12.2	−3.4	−3.8	−2.8	4.0
4	1915	7	2.59	22.8	11.1	11.7	−4.6	4.7	−1.9	8.0
5	1951	6	2.42	21.7	8.3	13.4	−2.9	−2.4	−1.1	6.0
6	1993	7	2.38							
7	1958	7	2.32	26.6	17.2	9.4	−2.3	−1.1	−1.3	3.0
8	1915	6	2.29	20.5	8.6	11.9	−3.3	6.3	−2.2	5.0
9	1915	8	2.24	25.5	14.4	11.1	−1.9	4.4	0.8	12.0
10	1947	6	2.17	22.2	10.5	11.6	−1.3	12.9	0.0	8.0
11	1916	6	2.08	21.2	8.9	12.2	−2.8	−4.4	−2.2	2.0
12	1950	7	1.89	27.2	12.8	14.4	−1.6	−2.7	−0.8	−3.0
13	1969	6	1.88	22.2	8.3	13.9	−2.6	−3.1	−3.3	−3.0
14	1993	6	1.80							
15	1905	7	1.70	25.5	13.3	12.2	−2.2	2.7	0.3	9.0
16	1982	6	1.59							
17	1977	8	1.59	24.4	8.9	15.5	−3.7	0.5	−3.6	−1.0
18	1911	8	1.54	24.4	11.1	13.3	−2.8	2.5	0.8	13.0
19	1974	8	1.50	25.5	8.8	16.7	−3.2	−0.5	−2.5	1.0
20	1912	8	1.39	25.5	12.2	13.3	−1.4	1.6	1.9	15.0

pling process intensifies the circulation within the South Dakota heat low. The heat low itself is important in dynamically contributing to amplify the maximum amplitude of temperature and precipitation fluctuations and radiatively driven enhanced sinking, in turn, enhancing lower tropospheric convergence south of Kansas City, which helps to cut off the moisture flow into the Mississippi valley. The associated westward displaced Bermuda high enhances this entire mechanism by also suppressing moisture convergence into the Mississippi valley plus enhancing warm flow into the Dakotas.

As reanalysis products improve, so will our observationally based understanding of Great Plains droughts. In the meantime, improved GCM simulations using characteristic land surface features along with realistic atmospheric initial conditions that generate the characteristic teleconnection patterns over the Northern Hemisphere might help to shed light on the partitioning between natural causes and anthropogenic causes, particularly as they pertain to drought initiation, maintenance, and withdrawal.

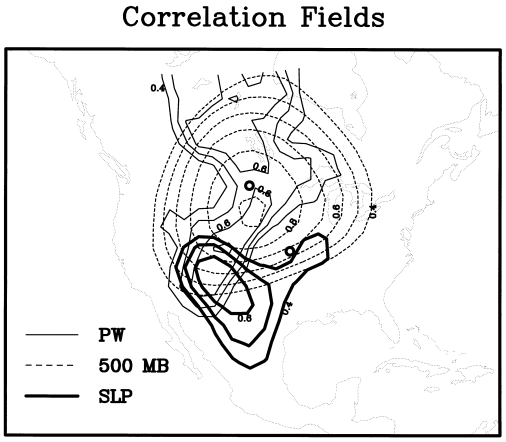

FIG. 19. Summary chart for correlations of SLP (thick solid lines), 500-mb geopotential height (dashed lines), and PW (thin solid lines) to drought index over U.S. Great Plains. Two small circles indicate Kansas City and Bismarck.

Acknowledgments. This research stems from the first author's Ph.D. dissertation, which has been supported by the Climate Dynamics Program of the National Science Foundation under Grant ATM-8318853. She is indebted to Professor John M. Wallace of the University of Washington for his scientific mentoring. A number of professors and colleagues have contributed to the success of this research during the last two decades. They are Professors James R. Holton and Dennis Hartmann of the University of Washington and Drs. Eugene Rasmusson, K.-M. Lau, C.-H. Sui, John Christy, Richard McNider, Pete Robertson, and Gary Jedlovec. The second author has been supported under an IPA assignment to the NASA Marshall Space Flight Center, Global Hydrology and Climate Center. He is also supported by NOAA GCIP Grant GC99-473. Last, but not least, the first author thanks Dr. Tina Chen of the Computer Science Corporation for providing her a comfortable private environment in which to revise the manuscript.

REFERENCES

Atlas, R., N. Wolfson, and J. Terry, 1993: The effect of SST and soil moisture anomalies on GLA model simulations of the 1988 U.S. summer drought. *J. Climate,* **6,** 2034–2048.

Betts, A. K., J. H. Ball, A. C. M. Beljaars, M. J. Miller, and P. A. Viterbo, 1996: The land surface–atmosphere interactions: A review based on observational and global modeling perspectives. *J. Geophys. Res.,* **101,** 7209–7225.

Bretherton, C., C. Smith, and J. M. Wallace, 1992: An intercomparison of methods for finding coupled patterns in climate data. *J. Climate,* **5,** 541–560.

Broomhead, D. S., and G. P. King, 1986: Extracting qualitative dynamics from experimental data. *Physica,* **20,** 217–236.
Chang, F.-C., 1986: On the seasonality of climate fluctuations over the contiguous United States. Ph.D. Dissertation, University of Washington, Seattle, WA, 161 pp.
——, and J. M. Wallace, 1987: Meteorological conditions during heat waves and droughts in the United States Great Plains. *Mon. Wea. Rev.,* **115,** 1253–1269.
Charney, J. G., 1975: Dynamics of deserts and drought in the Sahel. *Quart. J. Roy. Meteor. Soc.,* **101,** 193–202.
——, W. J. Quirk, S-H. Chow, and J. Kornfield, 1977: A comparative study of the effects of albedo change on drought in semi-arid regions. *J. Atmos. Sci.,* **34,** 1366–1385.
Currie, R. G., 1979: Distribution of solar cycle signal in surface air temperature over North America. *J. Geophys. Res.,* **84,** 753–761.
Douglas, M. W., 1995: The summertime low-level jet over the Gulf of California. *Mon. Wea. Rev.,* **123,** 2334–2347.
——, R. A. Maddox, K. Howard, and S. Reyes, 1993: The Mexican monsoon. *J. Climate,* **6,** 1665–1677.
Guttman, L., 1954: Some necessary conditions for common factor analysis. *Psychometrika,* **19,** 149–161.
Holopainen, E. O., 1970: An observational study of the energy of the stationary disturbance in the atmosphere. *Quart. J. Roy. Meteor. Soc.,* **96,** 626–644.
Horel, J. D., 1981: A rotated principal component analysis of the interannual variability of the Northern Hemisphere 500 mb height field. *Mon. Wea. Rev.,* **109,** 2080–2092.
Kalnay, E., M. Kanamitsu, and W. E. Baker, 1990: Global numerical weather prediction at the National Meteorological Center. *Bull. Amer. Meteor. Soc.,* **71,** 1410–1428.
——, and Coauthors, 1996: The NCEP/NCAR 40-Year Reanalysis Project. *Bull. Amer. Meteor. Soc.,* **77,** 437–471.
Kanamitsu, M., and Coauthors, 1991: Recent changes implemented into the global forecast system at NMC. *Wea. Forecasting,* **6,** 425–435.
Karl, T. R., and R. G. Quayle, 1981: The 1980 summer heat wave and drought in historical perspective. *Mon. Wea. Rev.,* **109,** 2055–2073.
——, C. N. Williams, P. J. Young, and W. M. Wendland, 1986: A model to estimate the time of observation bias associated with monthly mean maximum, minimum and mean temperatures for the United States. *J. Climate Appl. Meteor.,* **25,** 145–160.
Kerr, R. A., 1989: Hansen versus the world on the greenhouse threat. *Science,* **244,** 1041–1043.
Klein, W. H., 1952: The weather and circulation of June 1952: A month with a record heat wave. *Mon. Wea. Rev.,* **80,** 99–104.
Koster, R. D., and M. J. Suarez, 1995: Relative contributions of land and ocean processes to precipitation variability. *J. Geophys. Res.,* **100,** 13 775–13 790.
Kutzbach, J. E., 1967: Empirical eigenvectors of sea level pressure, surface temperature and precipitation complexes over North America. *J. Appl. Meteor.,* **6,** 791–802.
Labitzke, K., 1987: Sunspots, the QBO, and the stratospheric temperature in the north polar region. *Geophys. Res. Lett.,* **14,** 535–537.
——, and H. van Loon, 1992: Association between the 11-year solar cycle and the atmosphere. Part V: Summer. *J. Climate,* **5,** 240–251.
Lean, J., and D. Rind, 1998: Climate forcing by changing solar radiation. *J. Climate,* **11,** 3069–3094.
Lorenz, E., 1956: Empirical orthogonal functions and statistical weather prediction. Scientific Rep. No. 1, NTIS AD 110268 M.I.T. Statistical Forecasting Project, 49 pp.
Madden, R. A., and J. Williams, 1978: The correlation between temperature and precipitation in the United States and Europe. *Mon. Wea. Rev.,* **106,** 142–147.
Mintz, Y., 1984: The sensitivity of numerically simulated climates to land-surface boundary conditions. *The Global Climate,* J. T. Houghton, Ed., Cambridge University Press, 79–106.
Namias, J., 1982: Anatomy of Great Plains protracted heat waves (especially the 1980 U.S. summer drought). *Mon. Wea. Rev.,* **110,** 824–838.
——, 1991: Spring and summer 1988 drought over the contiguous United States—causes and prediction. *J. Climate Appl. Meteor.,* **22,** 30–39.
Naujokat, B., 1986: An update of the observed quasi-biennial oscillation of stratospheric winds over the Tropics. *J. Atmos. Sci.,* **43,** 1873–1877.
NCDC, 1994: Time bias corrected divisional temperature–precipitation–drought data (Documentation for dataset TD-9640), 12 pp. [Available from DBMB, NCDC, NOAA, Federal Building, 37 Battery Park Ave. Asheville, NC 28801-2733.]
Nicolis, C., and G. Nicolis, 1984: Is there a climatic attractor? *Nature,* **311,** 529–532.
——, and ——, 1986: Evidence for climatic attractors. *Nature,* **326,** 523–524.
Palmer, T. N., and C. Brankovic, 1989: The 1988 U.S. drought linked to anomalous sea surface temperature. *Nature,* **338,** 554–557.
Palmer, W. C., 1965: Meteorological drought. *Res. Pap. No. 45,* U.S. Weather Bureau, Washington, D.C., 58 pp. [Available from Library and Information Services Division, NOAA, Washington, D.C. 20852.]
Parrish, D. F., and J. C. Derber, 1992: The National Meteorological Center's spectral statistical interpolation analysis system. *Mon. Wea. Rev.,* **120,** 1747–1763.
Peixöto, J. P., and A. H. Oort, 1992: *Physics of Climate.* American Inst. of Physics, 500 pp.
Rasmusson, E., 1968: Atmospheric water vapor transport and the water balance of North America. Part II Large-scale water balance investigations. *Mon. Wea. Rev.,* **96,** 720–734.
——, 1997: North American hydrology: The evolution of an interdisciplinary perspective. *Bull. Amer. Meteor. Soc.,* **78,** 1187–1197.
——, P. A. Arkin, W-Y Chen, and J. B. Jalickee, 1981: Biennial variations in surface temperature over the United States as revealed by a singular decomposition. *Mon. Wea. Rev.,* **109,** 587–598.
Stockton, C. W., and D. M. Meko, 1983: Drought recurrence in the Great Plains as reconstructed from long-term tree-ring records. *J. Climate Appl. Meteor.,* **33,** 17–29.
Sud, Y. C., and M. J. Fennessy, 1982: A study of the influence of surface albedo on July circulation in semi-arid regions using the GLAS GCM. *J. Climatol.,* **2,** 105–125.
——, and ——, 1984: Influence of evaporation in semi-arid regions on the July circulation: A numerical study. *J. Climatol.,* **4,** 383–398.
Tang, M., and E. M. Reiter, 1984: Plateau monsoons of the Northern Hemisphere: A comparison between North America and Tibet. *Mon. Wea. Rev.,* **112,** 617–637.
Ting, M., and H. Wang, 1997: Summertime U.S. precipitation variability and its relationship to Pacific sea surface temperature. *J. Climate,* **10,** 1853–1873.
Trenberth, K. E., and G. W. Branstator, 1992: Issues in establishing causes of the 1988 drought over North America. *J. Climate,* **5,** 159–172.
——, and C. J. Guillemot, 1996: Physical processes involved in the 1988 drought and 1993 floods in North America. *J. Climate,* **9,** 1288–1298.
——, G. W. Branstator, and P. A. Arkin, 1988: Origins of the 1988 North American drought. *Science,* **242,** 1640–1645.
Vautard, R., and M. Ghil, 1989: Singular spectrum analysis in nonlinear dynamics, with applications to paleoclimatic time series. *Physica D,* **35,** 395–424.
Wallace, J. M., 1983: The climatological mean stationary waves: Observational evidence. *Large-Scale Dynamical Processes in the Atmosphere,* B. J. Hoskins and R. P. Pearce, Eds., Academic Press, 27–53.
——, and D. S. Gutzler, 1981: Teleconnections in the geopotential height field during the Northern Hemisphere winter. *Mon. Wea. Rev.,* **109,** 784–811.
——, C. Smith, and C. S. Bretherton, 1992: Singular value decomposition of wintertime sea surface temperature and 500-mb height anomalies. *J. Climate,* **5,** 561–576.
White, G. A., 1980: On the observed spatial scale of Northern Hemisphere transient motions. *J. Atmos. Sci.,* **37,** 892–894.